

DRAFT VERSION FEBRUARY 21, 2022  
 Typeset using **LATEX** **preprint** style in AASTeX631

## ROME III. The Arecibo Search for Auroral Emissions and Star-Planet Interactions at 5 GHz

MATTHEW ROUTE<sup>1, 2, 3, 4</sup> AND ALEX WOLSZCZAN<sup>1, 2</sup>

<sup>1</sup>*Department of Astronomy and Astrophysics, the Pennsylvania State University, 525 Davey Laboratory, University Park, PA 16802*

<sup>2</sup>*Center for Exoplanets and Habitable Worlds, the Pennsylvania State University, 525 Davey Laboratory, University Park, PA 16802*

<sup>3</sup>*Northrop Grumman Electronic Systems, 6120 Longbow Drive, Boulder, CO 80301*

<sup>4</sup>*Research Computing, Purdue University, 155 S. Grant St., West Lafayette, IN 47907, USA*

### ABSTRACT

Despite many attempts to detect radio emissions from magnetized exoplanets, a reproducible, unambiguous detection remains elusive. On the other hand, the search for periodic radio emissions from exoplanet host stars that may be induced by star-planet interactions in, for example, hot Jupiter systems, has only recently begun. In this third paper of the ROME (Radio Observations of Magnetized Exoplanets) series, we present the results of a targeted radio survey of 17 nearby systems that host exoplanet, brown dwarf, and low-mass stellar companions conducted with the Arecibo radio telescope at  $\sim$ 5 GHz. This GHz-frequency survey has the greatest frequency coverage of any to date, while providing mJy-level sensitivity over  $< 1$  s integration times. Neither auroral radio emissions from the substellar targets, nor exoplanet-induced stellar radio bursts were detected. These results are considered within the context of observed brown dwarf radio emissions, which support magnetospheric phenomenon similar to that found at Jupiter. We also describe the orbital phase coverage of our data for systems that may feature star-planet interactions, and briefly examine our results within the context of other searches for star-planet interactions within the same systems. Finally, as several of our targets are within their respective systems' habitable zones, we consider the implications of our survey on the search for technosignatures within those systems.

*Keywords:* Star-planet interactions; Magnetospheric radio emissions; Exoplanets; Planetary magnetospheres; Stellar activity; Non-thermal radiation sources

### 1. INTRODUCTION

While searching for radio emissions from the Crab Nebula (M1), Burke & Franklin (1955) serendipitously discovered radio emission from Jupiter. These emissions occurred at frequencies  $\leq$ 38 MHz, and were found to be highly elliptically polarized (Barrow & Morrow 1968). Several decades of both

Corresponding author: Matthew Route  
 mroute@ieee.org

remote and *in situ* observations of the Jovian magnetosphere have revealed that these early radio signatures were just one component of a legion of radio emissions caused by several processes and emission mechanisms. From 74 MHz to  $\gtrsim$ 20 GHz, Jupiter emits decimetric (DIM) synchrotron radiation from its magnetic poles and magnetic equator. These emissions are  $\sim$ 20% linearly polarized with circular polarization fractions that vary  $\pm$ 0.5% with rotational phase. The first radio signals detected from Jupiter were components of the decametric (DAM) emission, which ranges from 4 to 40 MHz. These emissions are  $\sim$ 100% circularly polarized with helicity and cutoff frequency of emission dependent upon which magnetic pole is observed. Some of the DAM activity is modulated by Io's and Ganymede's orbits. All DAM emissions, independent of source, are generated by the electron cyclotron maser (ECM) acting in the polar regions of the planet. The ECM also causes hectometric (HOM) emission, which is observed from  $\sim$ 400 kHz to  $\sim$ 4 MHz, and also is strongly circularly polarized. From  $\sim$ 20 kHz to 400 kHz, sporadic broadband (bKOM) and narrowband (nKOM) kilometric radiation are observed, which are generally linked to the propagation of ECM emission through the Io plasma torus. Within the 3.5 to 23 kHz frequency window, quasiperiodic emissions have been detected that appear as enhancements of continuum radio emissions. These continuum emissions span  $\sim$ 100 Hz to 25 kHz and are emitted in the ordinary mode. Among these components, the most powerful radio emissions are the DAM, HOM, and rapid S-bursts caused by coherent radiation processes; they are  $\sim$ 10<sup>5</sup> more luminous than the weakest emission, incoherent DIM (Zarka et al. 2004; Treumann 2006; de Pater & Lissauer 2015). It is therefore prudent that any search for auroral radio emissions from exoplanets should focus on detecting the signatures of ECM emission processes within their magnetospheres.

Beyond the Solar System, Yantis et al. (1977) sought to detect the first extrasolar planets via their Jovian-like radio emissions. Although their survey of 22 star systems failed to detect any candidates, it nevertheless served as a template for numerous subsequent survey efforts at radio frequencies (for a review see, for example, Lazio (2018)). These efforts sought to directly detect auroral radio emissions from the exoplanets following the examples of Jupiter and the other magnetized planets in the Solar System (e.g., Zarka (1998)).

In order to identify the most promising targets for surveys, numerous papers sought to estimate the radio flux density and frequency of exoplanetary radio emissions (e.g., Lazio et al. (2004); Griessmeier et al. (2007); Ignace et al. (2010); Reiners & Christensen (2010); Nichols (2012); Zaghou & Collins (2018)). Important ingredients in estimating the radio flux density are properties of the stellar wind (density, velocity, and interplanetary magnetic field), while exoplanet age, mass, and rotation rate are important determinants of the magnetic field strength (e.g., Christensen (2010)). The type of interaction that occurs between host stars and exoplanets are determined by whether the planet is strongly magnetized, or weakly/unmagnetized, leading to kinetic, magnetic, and unipolar interactions (e.g., Zarka (2007)). The first two types lead to the stellar-wind induced auroral emissions at Jupiter, while the last is exemplified by the Jupiter-Io system. Within the star-planet interaction context, it is possible that exoplanets orbiting close to their host stars, also known as hot Jupiters, may induce increased activity in their chromospheres, transition regions, and coronae via unipolar induction.

Cuntz et al. (2000) hypothesized that tidal and magnetic interactions between host stars and exoplanets with semimajor axes  $d \lesssim 0.1$  AU would increase stellar activity in several ways. First, tidal bulges would cause expansion and contraction of the outer layers of the stellar atmosphere, increas-

ing turbulent and flow velocities, and thereby increasing the energy available to generate acoustic and magnetic waves. In addition, increased turbulence may enhance dynamo activity within the convective zone, such as the subsurface  $\alpha$ -effect or turbulent dynamos. It is also possible that  $\alpha$ -enhancement may be transmitted to the tachocline at the bottom of the convective zone, leading to an overall enhancement of stellar activity throughout the stellar atmosphere. Independent of tidal effects, the star-planet interaction between exoplanet and host star may be magnetic, featuring stellar active regions that interact with exoplanet magnetospheres, enhancing processes such as coronal magnetic reconnection. Magnetic and tidal effects should be distinguishable by the presence of either one or two enhancements in activity per stellar rotation period, respectively. Note that both tidal and magnetic effects should be most pronounced in the corona and transition region, and to a lesser extent the chromosphere, due to their comparatively lower densities and proximity to the interacting substellar companion (Saar & Cuntz 2001).

Some observational support for this scenario comes from a chromospheric enhancement monitoring campaign conducted by Shkolnik et al. (2005). Several data sets of Ca II K residuals collected over two years from HD 179949 and  $\nu$  And may show enhanced activity at the  $\sim 1\%$  level, phased with the orbital period of the closest orbiting planet. However, the degree of modulation varies from epoch to epoch, with 25% of the epochs showing modulation of  $\lesssim 0.005\%$ . In addition, while planetary orbital phases of  $\phi_{orb}=0$  and potentially  $\phi_{orb}=0.5$  might be expected to produce enhanced activity in the above paradigm, Shkolnik et al. (2008) suggested that a more complicated energy transport model would be required to explain the enhanced activity found at  $\phi_{orb}=0.8$  to 0.95 in the case of HD 179949 and  $\phi_{orb}=0.53$  for  $\nu$  And. These works suggested that several additional exoplanets may interact with their host stars, such as HD 189733b. On the other hand, other research programs have failed to find a statistically significant correlation between exoplanets with small semimajor axes and chromospheric activity enhancement (e.g., Canto Martins et al. (2011)).

Rubenstein & Schaefer (2000) hypothesized that as-yet undetected planetary companions could cause the emission of superflares ( $E \sim 10^{33}$ - $10^{38}$  ergs) from F and G main-sequence stars. They argued that the properties of flares emitted from  $\kappa$  Ceti and  $\pi^1$  UMa were similar to those emitted by RS Canum Venaticorum (RS CVn) stars. They suggested that open field lines from the host star were anchored at the exoplanetary companion. The magnetic field strength would be amplified by a wrapping of magnetic field lines as the exoplanet orbits the star, and subsequent interactions of magnetic loops between the star and planet would result in magnetic reconnection events that would trigger superflares. They further hypothesized that these flares would be luminous at X-ray to radio wavelengths, in analogy to RS CVn and solar flares.

Therefore, a useful lens through which to search for and observe stellar activity is at radio wavelengths, which provide powerful diagnostics of coronal flaring and shock processes that may be induced or enhanced by star-planet interactions. In addition to manifesting another aspect of coronal activity, radio emissions provide information on plasma density, local magnetic field, particle acceleration, and wave propagation processes for a number of stars (e.g., Benz & Güdel (2010)). The best studied amongst these is obviously the Sun, which, due to its proximity, enables for the study of magnetic activity at great sensitivity with high spatial and temporal resolution. Against a background of thermal bremsstrahlung emission, both incoherent gyrosynchrotron and coherent emissions processes contribute. At mm to cm wavelengths, gyrosynchrotron dominates, while at dm to m wavelengths, coherent plasma radiation dominates (Bastian et al. 1998). Another coherent emission mechanism,

ECM, may cause solar radio emissions with narrowband components, such as the fine structure within Type IV bursts and solar microwave spikes. The frequencies of emission of these two phenomena range from  $\sim$ 50 MHz to 10 GHz for the former and  $\sim$ 100 MHz to 5 GHz for the latter (Treumann 2006; Pick & Vilmer 2008). Dulk (1987) summarized how these four radio emission mechanisms - thermal bremsstrahlung, gyrosynchrotron, plasma, and electron cyclotron maser - differ in terms of their brightness temperatures,  $T_B$ , circular polarization fractions, and timescales of variability in addition to their operation in differing frequency domains. Observations at 5-10 GHz are especially promising, as microwave bursts generated by gyrosynchrotron emission tend to peak within this frequency window, and several types of ECM-generated activity are also present.

Given these currents in research within the community, we conducted a survey of nearby star systems with known substellar companions at Arecibo Observatory (AO) in 2010-2011. A detailed account of the analysis and interpretation of one exoplanet system that we surveyed, HD 189733, has recently been presented in ROME I (Route 2019) and ROME II (Route & Looney 2019). In Section 2, we describe our target selection methodology, instrumentation, and observations. In Sections 3 and 4, we present the results of our survey, and contextualize these results both in terms of ultracool dwarf (UCD) radio activity, and star-planet interactions. In the latter section, we also discuss the implications of our results on the search for direct emissions from exoplanets and potential civilizations within their habitable zones (HZs). Finally, we conclude by reviewing the significance of this survey and providing suggestions for future work in Section 5. Together, these results and considerations indicate that the direct detection of exoplanet auroral emissions, and their indirect detection and characterization via star-planet interactions remains an admirable, although difficult, goal.

## 2. TARGET SELECTION AND OBSERVATIONS

### 2.1. *Target Selection*

Survey targets were chosen based on two classes of factors: the physical properties of the systems and their location in the sky (Table 1). We targeted stars with substellar companions thought to be exoplanets at the time that were  $<50$  pc from the Sun. This was necessary because even for the most optimistic estimates of their emitted auroral radio flux (e.g., Lazio et al. (2004)), they would still be marginally detectable if observed at the cutoff frequency of their emission. Similarly, stellar coronal flare luminosities follow a power-law distribution (e.g., Güdel et al. (2003)), so that increasingly distant sources require stronger, and rarer, star-planet induced flares for detection.

We further constrained our sources by mass and semi-major axis: over three quarters of our targets are  $<0.5$  au from their host stars and over half of our targeted systems have an orbiting companion  $>3 M_J$ . Exoplanets close to their parent stars were preferred because they are hypothesized to have greater radio luminosity due to the greater dissipated kinetic or magnetic power from the stellar wind impinging on their magnetospheres (Zarka 2007). Eight of our chosen planetary systems are within the semimajor axis range  $a \lesssim 0.1$  au considered by Cuntz & Shkolnik (2002) to be especially promising for the detection of enhanced activity caused by star-planet interactions, including 51 Peg b and HD 209458b which both appeared in their study.

We selected larger exoplanet masses because theoretical models suggest that these planets have greater thermal flux available to power convection-driven magnetic dynamos, resulting in larger mean magnetic field strengths (Christensen et al. 2009; Reiners & Christensen 2010). We note that in many cases, the quantity  $M \sin i$ , as opposed to the true mass, is measured for substellar compan-

ions, resulting in an uncertain classification as exoplanets based on their minimum potential masses. However, given geometric effects due the ambiguity in the orbital inclination angle,  $i$ , the true mass of a companion is typically  $\sim 15\%$  higher<sup>1</sup> (e.g., [Reffert & Quirrenbach \(2011\)](#)). We therefore targeted HD 38529b (now HD 38529c) and HD 114762 Ab as candidates that potentially straddle the exoplanet/brown dwarf boundary, despite having reported masses of 12.7 and 11  $M_J$ , respectively ([Latham et al. 1989](#); [Fischer et al. 2003](#)). In these latter cases, their radio emission may be quite strong and at  $\sim 4\text{--}5$  GHz frequencies as it is for the  $\sim 900$  K, T6.5 brown dwarf 2MASS J10475385+212434 (J1047+21; [Route & Wolszczan \(2012\)](#)).

Finally, the single, fixed-dish nature of the Arecibo radio telescope required our targets to have declinations of  $0^\circ$  to  $+38^\circ$ .

## 2.2. *Instrumentation and Observations*

The exoplanet targets comprised approximately half of the objects surveyed during AO program A2471, conducted from 2010 January 8 to 2011 September 6; the other half were UCDs of spectral types  $\geq M7$ , with results presented in [Route & Wolszczan \(2012, 2013\)](#). Each exoplanetary system was observed for a total of 40 mins to 2.5 hrs, sometimes across multiple epochs, although no single epoch was longer than 2 hrs (Table 2). The  $\sim 2$  hr observing session limitation represents the maximum time for a target to transit the field of view of the fixed dish of the Arecibo radio telescope. During these observing sessions, 20-sec calibration on-off scans using a local oscillator were interlaced between 10-minute target scans.

Although the 305 m dish is fixed, the William E. Gordon radio telescope at AO offered several advantages relative to other facilities, including its exquisite sensitivity, accurate polarization measurements over short time scales, and large,  $\sim 1$  GHz bandpass, which was exemplary in 2010-2011. The observing system consisted of the C-band receiver<sup>2</sup> and the recently commissioned Mock spectrometer<sup>3</sup>. The system temperature ranged from 25–32 K, with antenna gains of  $5.5\text{--}9.0$  K Jy $^{-1}$ . The half-power beam width varied from  $0.97 \times 1.09$  arcmin (azimuth  $\times$  zenith angle) at 4500 MHz central frequency to  $0.79 \times 0.92$  arcmin at 5400 MHz (Chris Salter, personal communication). Full Stokes parameters were computed by the Mock spectrometer array based on the dual-linear polarization input signals from the receiver. This array consists of seven field-programmable gate array (FGPA) Fast Fourier Transform (FFT) Mock spectrometers, which were individually tuned to central frequencies of 4325, 4466, 4608, 4750, 4892, 5034, and 5176 MHz, resulting in a  $\sim 1$  GHz simultaneous bandpass stretching from 4239 to 5262 MHz. Although each 8192-channel spectrometer permits a 172 MHz bandpass, in practice edge effects reduce the usable bandpass to  $\sim 140$  MHz ([Salter 2009](#)). The spectrometer data were sampled in 0.1 s intervals.

Prior to analysis, data were resampled at 83.6 kHz and 0.9 s frequency and temporal resolutions, respectively, to improve the signal-to-noise ratio. Radio frequency interference (RFI) was reduced through an iterative statistical process detailed in ([Route 2013](#)). The  $1\sigma$  instrumental sensitivity was  $\sim 0.1\text{--}1.2$  mJy, with per-scan sensitivity distribution properties described in ([Route 2017b](#)). Data analysis consisted of the creation of dynamic spectra (time-frequency spectrograms) and time series graphs of flux density in each polarization across all spectrometers. Since one of the hallmarks of the two most likely types of radio emission, ECM and gyrosynchrotron, is significant circular

<sup>1</sup> “Exoplanets Data Explorer | Table,” available at <http://exoplanets.org/table>

<sup>2</sup> “C-Band,” available at <http://www.naic.edu/~astro/RXstatus/Cband/Cband.shtml>

<sup>3</sup> “The ‘Mock’ Spectrometer,” <http://www.naic.edu/%7Eastro/guide/node9.html>

polarization, we searched Stokes V dynamic spectra for  $\gtrsim 10\%$  bursts of emission that did not have accompanying Stokes U and V counterparts. AO is insensitive to quiescent radio emission due to its local calibration procedure and confusion limitations, thus, only circularly polarized radio bursts of several minutes' duration could be detected. However, this may not be a major limitation of our observing methodology since both Jupiter and Uranus emit bursts of radio emission in addition to their smooth components (Zarka 1998).

### 3. RESULTS

#### 3.1. *Direct Search for Radio Emission from Companion Objects*

No radio bursts of any type were detected from any system hosting exoplanet or brown dwarf companions. We reiterate that this survey was sensitive only to  $\gtrsim 10\%$  circularly polarized bursts of radio emission of several minutes duration, and this survey was entirely insensitive to quiescent and/or non-polarized emission from the systems observed. Due to the angular resolution of the beam, this result means that for each targeted system, no radio emission was directly detected from exoplanets within the system, nor was host star radio emission induced by tidal or magnetic effects from the closest exoplanets detected.

However, we can place upper limits on circularly polarized radio emission from the systems studied by computing the standard deviation of the frequency-integrated time series of the cleanest Mock spectrometer, centered at 4466 MHz. For complete results of the frequency-dependent sensitivity of observations on a system-by-system basis, see Route (2013). Table 3 lists the  $3\sigma$  upper limits on the detection of radio emission from the exoplanet systems observed. A comparison of these detection limits to several types of flares is depicted in Figure 1, and Figure 2 displays the detection limits from this survey compared to other surveys of UCDs. We note that these upper limits provide tighter constraints on target radio emission than in the sister surveys of UCD radio activity conducted with the same instrumental set up and analysis software, due to the quieter radio environment around AO in 2010-2011 (Route 2013; Route & Wolszczan 2013, 2016b).

##### 3.1.1. *Companion Bolometric Luminosities*

It is common in the substellar community to report the radio emission from targets as a fraction of their bolometric luminosities. There are several ways to obtain these luminosities. High-contrast near infrared imaging and spectroscopy enable a direct measurement of the bolometric luminosities of the members of the HR 8799 system (Marois et al. 2010; Brandt et al. 2021). The revised determination of the mass of HD 114762 Ab enables us to estimate its spectral type (M5) and, therefore, its bolometric luminosity (Reid & Hawley 2005; Kiefer et al. 2021). For a limited number of transiting exoplanets (55 Cnc e, HD 189733b), we leverage direct measurements of their radii and effective temperatures to determine their bolometric luminosities via the Stefan-Boltzmann equation.

However, in most cases, the radii and effective temperatures of the companion objects are unknown. For many substellar companions, the radii are estimated from the mass-radius relationships found in Figures 1 and 2 of Chabrier et al. (2009) for companions with  $M \geq 1 M_J$ , and in Figure 4 of Seager et al. (2007) for companions of sub-Jupiter mass. When direct measurements of effective temperatures exist (HD 10697b, 55 Cnc e, HD 189733b) we have averaged their day and nightside temperatures. Next, when available, we use effective temperatures reported in the literature. For the remaining cases ( $\epsilon$  Tau b; GJ 176b; HD 38529b; HD 50544b; 55 Cnc b, c, and d; HD 102195b; 70 Vir b; HD 178011 Bb; HD 195019b) we can crudely estimate the equilibrium effective temperatures

by following the prescription in Marcy & Butler (1996):

$$T_{eff} \approx T_*(R_*/2a)^{1/2}(1 - A)^{1/4}, \quad (1)$$

where  $T_*$  and  $R_*$  are the effective temperature and radius of the host star, respectively,  $a$  is the companion semimajor axis, and  $A$  is the Bond albedo of the companion, which is assumed to be  $\sim 0.35$  as it is for Jupiter. The measured and computed bolometric luminosity for each companion is given in Table 4, and its computed  $\nu L_\nu/L_{bol}$  is listed in Table 3.

An alternative method would use evolutionary models for cool brown dwarfs and giant planets ( $M \geq 0.5 M_J$ ) (e.g., Baraffe et al. (2003)). However, given that both isolated and irradiated models appear to systematically underestimate the bolometric luminosities of exoplanets (e.g., HD 209458b) we have opted not to use them here. Nevertheless, we note that were these models to be used, for system ages of  $\sim 5$  Gyr, the modeled bolometric luminosities differ by 0.0 to -6.4 dex. Thus, in general, evolutionary models systematically shift nearly all points upward in  $\nu L_\nu/L_{bol}$  in Figure 3.

### 3.2. Orbital Phase Coverage of Companions for Star-Planet Interactions

We next evaluate the constraints placed on the occurrence of star-planet interactions within the systems we targeted. Borrowing from nomenclature for hot Jupiters, we first divide our sample into targets with hot exoplanets ( $P < 10$  d), warm exoplanets ( $10 \leq P < 200$  d), and longer period targets (e.g., Dawson & Johnson (2018)). For “hot” and “warm” exoplanets, we compute the orbital phase coverage of our observations using

$$T_0 = T_t + P E_{orb}, \quad (2)$$

where  $T_0$  represents the beginning or end of the observation,  $T_t$  represents the measured (or estimated) midpoint of transit (or periapse),  $P$  is the exoplanet orbital period, and  $E_{orb}$  is the orbital cycle. Orbital phase 0.0 denotes when transit or periapse would occur.

The results for “hot” targets are reported in Table 5. Even among the shortest-period exoplanets, our orbital phase coverage is quite modest since many targets were observed for  $\sim 1$  hr, and only three targeted systems for  $> 1.5$  hr. The peak orbital phase coverage ( $\Delta\phi_{orb} = 0.08$ ) occurs for 55 Cnc e, although the coverage and timing of the observations for HD 189733 is also significant (Section 4.1.7). Among “warm” targets, the maximum coverage is  $\Delta\phi_{orb} = 0.004$  for 55 Cnc b and HD 195019b. More importantly, however, even the warm Jupiter closest to its host star, HD 195019b ( $a = 21.62 R_*$ ), is too far away to induce enhanced stellar activity through magnetic and tidal star-planet interactions. In summary, despite the excellent sensitivity of AO, the modest orbital phase coverage only loosely constrains the incidence of star-planet interactions within the observed systems.

## 4. DISCUSSION

### 4.1. Companion Objects of Special Interest

#### 4.1.1. HD 114762 Ab

In Section 2.1, we noted that the measurement of  $M \sin i$  via the radial velocity method leaves an ambiguity in the true mass of the object, which can lead to a corresponding underestimate of its internal energy to power a convective dynamo. This would then result in an underestimate of the magnetic field strength of the substellar object, and accompanying searches at too low of frequencies.

While we did not detect radio emissions from any exoplanet candidate targeted by our survey, we highlight that several of our targets were subsequently reclassified as brown dwarfs or low-mass stars.

Given the updated mass estimate for HD 114762 Ab from [Kiefer et al. \(2021\)](#) and the mass-spectral type relationship depicted in Figure 10 of [Chabrier & Baraffe \(2000\)](#), we estimate that this companion is actually an M5 dwarf, as opposed to a  $\sim 11$   $M_J$  giant planet as originally thought ([Latham et al. 1989](#)). Although we did not detect any high brightness temperature, highly-circularly polarized ECM-generated radio flares from this system, these flares are common among M dwarfs. They have been observed in variety of M dwarf containing systems, including at 4.85 GHz from the M3.5 dwarf AD Leo ([Stepanov et al. 2001](#)) and potentially from the M5 companion in the “white dwarf pulsar” cataclysmic variable system AR Sco at 1-10 GHz ([Lyutikov et al. 2020](#)).

#### 4.1.2. *HD 38529 and HD 106252b*

Based on their radiometric Bode’s law, [Lazio et al. \(2004\)](#) estimated that if HD 38529c and HD 106252b were exoplanets, they would be sources of  $\Phi_{radio} \sim 13$   $\mu$ Jy and  $\Phi_{radio} \sim 32$   $\mu$ Jy radio emissions extending to cutoff frequencies of  $\nu \sim 1.6$  GHz and  $\nu \sim 576$  MHz, respectively. These estimates were based on the ability of their respective magnetospheres to dissipate incident stellar wind power. However, the revised mass estimates for HD 38529c and HD 106252b (Table 1) clearly place them in the brown dwarf domain ([Fritz Benedict et al. 2010](#); [Reffert & Quirrenbach 2011](#)). Using these revised masses together with 5 Gyr isochrone models ([Baraffe et al. 2003](#)) and the effective temperatures from [Cushing et al. \(2011\)](#), we estimate that HD 38529c and HD 106252b have spectral types of Y0 and T9, respectively. The 2010 observations of these two objects, therefore, constitute the first, although inadvertent, search for radio emission from potential Y dwarfs. Since the latest spectral type and coolest effective temperature for which radio emission has been discovered is from the  $T_{eff} \sim 900$  K J1047+21, which was a source of  $\Phi_{radio} \sim 3$  mJy radio emissions at  $\nu \gtrsim 4$  GHz ([Route & Wolszczan 2012](#)), these systems may also be sources of radio emission at  $\sim$ GHz frequencies and mJy flux densities. Unfortunately, both systems are  $\sim 4\times$  further away than J1047+21, so that while the instrumentation and techniques to search for radio emissions remain the same for all three objects, the upper limits for detectable radio emission from HD 38529c and HD 106252b are nearly an order-of-magnitude higher.

The HD 38529 system also contains a warm Jupiter, HD 38529b, which [Lazio et al. \(2004\)](#) predicted could be a source of  $\Phi_{radio} \sim 6$  mJy radio emission up to a cutoff frequency of  $\nu \sim 16$  MHz.

#### 4.1.3. *HD 46375*

[Lazio et al. \(2004\)](#) estimated that HD 46375b may be a source of  $\Phi_{radio} \sim 80$  mJy auroral radio emission up to a cutoff frequency of  $\nu \sim 0.6$  MHz, which is below the frequency threshold at which radio emissions can penetrate the terrestrial ionosphere. [Shkolnik et al. \(2005\)](#) searched for periodic, star-planet induced chromospheric variability in the Ca II H & K lines (3968 and 3933  $\text{\AA}$ ) among HD 46375 and several other program stars. No change was detected to a level of 0.001. Similarly, we did not detect exoplanet auroral emission or any sign of star-planet interactions in this system, although our observations only occur at  $\phi_{orb} \sim 0.68$ . This orbital phase is somewhat removed from  $\phi_{orb} \sim 0.5$ , which theory indicates may experience augmented activity due to tidal star-planet interactions.

#### 4.1.4. *70 Vir*

Lazio et al. (2004) anticipated that 70 Vir b would be a  $\Phi_{radio} \sim 2$  mJy source of auroral radio emissions at  $\nu \sim 546$  MHz, based on its ability to dissipate incident stellar wind power. Saar & Cuntz (2001) searched for star-planet induced chromospheric activity in the Ca II infrared triplet (IRT; 8662 Å) among several exoplanet-hosting systems, including 70 Vir. They found no variability down to  $\sim 3.5\%$ , and we found no evidence for coronal activity enhancement. We also did not directly detect radio emissions from any exoplanet auroral activity.

#### 4.1.5. 51 Peg

Lazio et al. (2004) and Reiners & Christensen (2010) estimated that 51 Peg b may emit  $\nu \sim 1.2$  MHz, or  $\nu \sim 7$  MHz, radio waves up to a level of  $\Phi_{radio} \sim 251$  mJy, or  $\Phi_{radio} \sim 0.8$  mJy, respectively. Both cutoff frequencies, however, are below the terrestrial ionospheric frequency threshold. Saar & Cuntz (2001) found no sign of star-planet interactions in the Ca II IRT down to  $\sim 3.2\%$ . Shkolnik et al. (2003) reported significant nightly activity for 51 Peg which they suggested might be cyclical and phase shifted based on  $\sim 10$  nights of Ca II H & K observations. Subsequent observations found no variability down to 0.001 (Shkolnik et al. 2005). While our observations are agnostic with respect to this prediction of auroral emissions, we found no evidence for star-planet induced coronal activity at  $\phi_{orb} \sim 0.22$ , nor at  $\phi_{orb} \sim 0.43$ , near the anticipated tidal activity enhancement zone.

#### 4.1.6. HD 209458

Lazio et al. (2004) used their radiometric Bode's law to predict that HD 209458b's auroral radio emission might peak at  $\nu \sim 2.9$  MHz with a flux density of  $\Phi_{radio} \sim 25$  mJy. As with other predictions where the cutoff frequency  $\nu < 10$  MHz, such emission would be undetectable from the ground due to reflection from the terrestrial ionosphere. As with 51 Peg b, preliminary monitoring of chromospheric Ca II H & K activity suggested nightly activity which could be periodic in nature, but was later found to lack variability down to the level of 0.001 (Shkolnik et al. 2003, 2005). Alternatively, Jensen et al. (2012) found an anomalous shifting of the broad component relative to the narrow component of the H $\alpha$  line in transmission spectra during transit and secondary eclipse. They suggested that stellar chromospheric activity enhanced by star-planet interactions may alter the H $\alpha$  line shape, although this phenomenon may also point to a data reduction artifact. Our radio observations do not find evidence of auroral activity, nor star-planet induced coronal activity within this system at  $\phi_{orb} \sim 0.01$  nor  $\phi_{orb} \sim 0.87$ . Note that enhanced activity near  $\phi_{orb} = 0.0$  would be anticipated in both tidal and magnetic interaction cases.

#### 4.1.7. HD 189733

The proximity of the HD 189733 system to the Earth, the brightness of the primary star, and fortuitous alignment of the hot Jupiter companion that result in a transit every 2.219 d have made the system a particularly inviting target for study. With a chromospheric activity index, S-value=0.525, HD 189733A is among the 10% most active K dwarfs in the the California and Carnegie Planet Search Project. Transmission spectroscopy of the frequent transits have resulted in the discovery of the exoplanet atmosphere's composition, thermal properties, and evaporation. Multiwavelength observations of the system have revealed a wealth of stellar activity from optical to X-ray wavelengths, including spots and flares at all rotational and exoplanetary orbital phases. Compellingly, several research groups announced the discovery of enhanced chromospheric, transition region, and coronal activity that may be phased with exoplanet orbital phases  $\phi_{orb} \sim 0.5\text{--}1.0$ , that may be caused by

magnetic and/or tidal star-planet interactions. In one case, it was furthermore suggested that the primary star may be actively accreting evaporated material from HD 189733b (see ROME I and references therein).

In ROME I, we analyzed AO radio observations to search for enhanced coronal activity associated with such star-planet interactions. We also analyzed *Microvariability and Oscillations of Stars (MOST)*, Automated Photoelectric Telescope (APT), and Wise photometry to search for periodicities suggestive of stellar hemispheres that contain more darkened starspots than average, that may point to enhanced photospheric activity associated with these interactions. We also compiled all observations and reported instances of stellar spotting and flaring at radio through X-ray wavelengths to attempt to discover enhancements phased to the orbital period of the exoplanet. Our results could find no statistically significant enhancement, including at the orbital phases that other research groups thought might suggest star-planet interactions. In ROME II, we again leveraged *MOST*, APT, and Wise photometry to search for photometric bright features that may be related to accretion structures, using the T Tauri paradigm as a template. After computing plasma parameters such as density, temperature, accretion rate, and flare structure sizes, we determined an accretion rate of  $\dot{M} \sim 10^9$  to  $10^{11}$  g s<sup>-1</sup>, which would result in undetectably low activity at all wavelengths. Since the publication of ROME II, new flare observations and several reanalyses of existing optical and UV data sets have been presented, which we will address in a forthcoming publication (e.g., [Bourrier et al. \(2020\)](#) and references therein).

However, for the purposes of this paper, we will remain focused on research that may directly influence the ability of HD 189733A or its exoplanet companion to produce radio emission. Based on their convective dynamo model, [Reiners & Christensen \(2010\)](#) estimated that HD 189733b would have a detectable radio flux density of  $\Phi_{radio} \sim 57$  mJy up to an ECM cutoff frequency  $\nu \sim 39$  MHz. [Zaghoo & Collins \(2018\)](#) used a revised interior conductivity profile to estimate peak ECM emission at  $\nu \sim 15$  MHz with a radio flux density of  $\Phi_{radio} \sim 20$  mJy. [Kavanagh et al. \(2019\)](#) leveraged the 3D magnetohydrodynamic modeling code BATS-R-US to investigate the prospects for the detection of radio emissions from HD 189733b. They used the magnetic field topology maps of HD 189733A derived from several epochs of ZDI observations from [Fares et al. \(2017\)](#) as inputs. They found that an exoplanetary polar magnetic field  $B \sim 10$  G would be required to create ECM emission at  $\nu \sim 25$  MHz that is higher than the plasma frequency of the stellar wind environment and thus could escape to an observer with  $\Phi_{radio} \sim 50$ -130 mJy. Our radio observations do not shed any light on these predictions as no exoplanet auroral activity was observed. We also find no evidence for star-planet induced coronal activity within this system at  $\phi_{orb} \sim 0.57$ –0.61 (ROME I).

#### 4.1.8. 55 Cnc

The 55 Cnc binary system consists of a K0 primary, an M4.5 secondary, and five exoplanets that circle the primary. The closest orbiting exoplanet, 55 Cnc e, has a sub-Neptune mass and may be close enough to its host star to cause star-planet interactions, although its magnetosphere would likely present a very small cross section for magnetospheric interactions. 55 Cnc f orbits within its host star's HZ, which will be discussed in more detail in Section 4.3. [Lazio et al. \(2004\)](#) estimated that 55 Cnc b, c, and d would be sources of radio emission up to cutoff frequencies of  $\nu \sim 17.6$  MHz, 1.7 MHz, and 242 MHz, with flux densities of  $\Phi_{radio} \sim 80$  mJy, 40 mJy, and 80  $\mu$ Jy, respectively. Unfortunately, no auroral emissions, nor star-planet induced coronal activity were observed in this system.

#### 4.1.9. *HD 195019b and HD 178911 Bb*

[Lazio et al. \(2004\)](#) suggested that the two warm Jupiters, HD 195019b and HD 178911 Bb may be sources of  $\Phi_{radio} \sim 16$  mJy, and  $\sim 0.63$  mJy auroral radio emissions up to cutoff frequencies of  $\nu \sim 184$  MHz, and  $\sim 504$  MHz, respectively. Unfortunately, we did not detect any signatures of exoplanet auroral emissions or star-planet interactions in these systems.

#### 4.1.10. *HD 10697 and HD 50554*

Leveraging their radiometric Bode's law, [Lazio et al. \(2004\)](#) predicted that HD 10697b and HD 50554b would produce auroral radio emissions at  $\nu \sim 545$  MHz and 333 MHz with flux densities of  $\Phi_{radio} \sim 80$  and  $63 \mu\text{Jy}$ , respectively. Although these exoplanets have relatively high masses and estimated cutoff frequencies, their  $a > 2$  au semimajor axes place them at a significant disadvantage in terms of dissipating incident solar wind power compared to our other targets. No auroral emissions were detected in these systems.

### 4.2. *Reasons for Non-Detections*

There are several potential reasons for the non-detection of radio emissions from the targeted systems, which must be assessed in light of both intrinsic exoplanet magnetospheric radio emissions, and star-planet induced coronal radio emissions. These reasons include sensitivity, observing frequency, observation durations, and viewing geometry.

#### 4.2.1. *Sensitivity*

Although this survey is the most sensitive to date, in many cases, the exoplanet auroral emissions would need to be  $\sim 10^6$  greater than those of Jupiter in order to be detectable (Table 3). By comparison, [Zarka \(2007\)](#) estimated that hot Jupiters might produce radio emissions  $10^3$  to  $10^6$  times more intense than those emitted by Jupiter based on their empirically derived radio-magnetic Bode's law. Somewhat less optimistically, [Lazio et al. \(2004\)](#) suggested that greater stellar wind loading among hot Jupiters would scale-up emissions analogous to Jovian peak power emissions by  $10^2$ . Our effort, then, is at the edge of viability with respect to these models.

Within the context of star-planet interactions, we note that ECM-induced stellar flaring would be detectable in nearly all cases (Figure 1), as was found in our study comparing the activity of HD 189733A to active M dwarf ECM flares (ROME I). Similar to the findings of that work, only the most luminous gyrosynchrotron flares might be visible from some targets within our survey. Unfortunately, the anticipated radio luminosity of flares (as derived from the X-ray emissions and the Güdel-Benz relationship) from isolated, active stars such as the K2V  $\epsilon$  Eri, does not exceed the detection thresholds for flares from our most sensitive observations. On the other hand, it is possible that the radio counterparts of the extremely luminous superflares observed in the optical may be visible from our survey ([Schaefer et al. 2000](#)). As mentioned in Section 1, it has been hypothesized that such flares may be powered by the magnetospheric interaction of close-in giant exoplanets. However, generally speaking, it is non-trivial to estimate the radio luminosity of flares based on their optical emissions alone (e.g., [Priest \(2014\)](#)). If such flares have radio luminosities comparable to their optical emission,  $L \sim 5 \times 10^{31}$  ergs  $\text{s}^{-1}$  would be readily detectable by our survey.

#### 4.2.2. *Observing Frequency and Magnetic Field Strengths*

Another important facet to consider is the frequency coverage of our survey. Since our survey was primarily sensitive to ECM emissions generated either by the direct exoplanet auroral emissions or exoplanet-induced stellar flaring, we will consider only this emission mechanism. The cutoff frequency of ECM radio emissions is related to the local cyclotron frequency,  $\nu_c$ , by  $\nu_c[\text{MHz}] = 2.8nB$  [Gauss], where  $n$  is the harmonic number, and  $B$  is the local magnetic field strength. Therefore, since we surveyed targets within the frequency range 4250 MHz to 5250 MHz, this corresponds to emission from magnetic fields of strength  $B \sim 1.5$  to 1.9 kG for emission at the fundamental frequency, and  $B \sim 760$  to 940 G at the second harmonic. Theoretical models indicate that both modes are possible, although which mode of emission dominates is dependent upon the local plasma conditions (Treumann 2006). We note that Trigilio et al. (2011) has found evidence for near-simultaneous radio emission in both modes from the magnetic chemically peculiar star CU Virginis. At first blush, the magnetic field ranges that correspond to the frequency range of our survey appear to be too high to be scientifically useful.

For the most part, radio surveys of exoplanets have sought emission at much lower frequencies. Only a handful of targets have traditionally been hypothesized to have  $\sim$ GHz radio emissions, such as HD 114762 Ab, HD 38529c (before their updated mass determinations), HD 43197b, PSR B1620-26 b, and WASP-77A b (Lazio et al. 2004; Sirothia et al. 2014). However, given the *Msini* mass ambiguity, if, for example, the mass of an object such as HD 38529c was underestimated by a factor of 1.8, this would correspond to an increase in its emission frequency of  $\sim 2.7$ , placing it within our survey range. Indeed, after the completion of our survey it was confirmed that HD 38529c, HD 106252b, and HD 114762 Ab were more massive than first thought, with the first two targets declared to be brown dwarfs and the last we estimate to be an M5 dwarf.

The primary component in the determination of the frequency of intrinsic radio emissions from substellar companions is their magnetic field strengths as governed by the internal energy available to power their convective magnetic dynamos. This internal energy can be estimated based on parameters such as mass, radius, age, rotation rate, and internal composition and conductivity. Figure 1 of Reiners & Christensen (2010) depicts the magnetic field evolutionary tracks for stars and substellar objects of various masses given the geodynamo scaling law devised by Christensen et al. (2009). From these models, the maximum magnetic field strengths found in  $\sim 1$  Gyr M dwarfs, brown dwarfs, and exoplanets, should be approximately 4 kG, 3 kG, and 200 G, respectively. However, there is some evidence that these models may, in fact, underestimate the magnetic dynamo strengths that can be achieved in these objects. Following our detection of a  $B \sim 1.7$  kG magnetic field from the  $\sim 900$  K, T6.5 brown dwarf J1047+21, additional observations at 10 GHz (Williams & Berger 2015) and 15.75 GHz (Kao et al. 2018) have suggested that this brown dwarf may host magnetic fields as strong as 5.6 kG, assuming ECM radiation at the fundamental frequency. Furthermore, the latter paper suggests that the T2.5 brown dwarf SIMP 01365662+0933473 may actually be a  $\sim 200$  Myr substellar object of only  $\sim 13$   $M_J$ , yet with a magnetic field strength  $B \sim 3.2$  kG.

Confirmation of these characteristics would imply that brown dwarfs and exoplanets maintain much stronger magnetic fields than anticipated, and will provide useful constraints to revise magnetic dynamo models. We reserve a more thorough discussion of dynamo scaling laws as applied to exoplanets and brown dwarfs for a later paper in the ROME series. However, these considerations indicate that it is not unreasonable to survey exoplanets at higher frequencies than traditionally assumed, given enough sensitivity. On the other hand, it is important to note the dynamo mod-

els of Christensen et al. (2009) and Reiners & Christensen (2010) require rapid rotation. Since the hot Jupiters surveyed may be tidally locked, the convective motions of their internal dynamos may be drastically reduced, resulting in diminished global dipolar magnetic fields (e.g., Sánchez-Lavega (2004)). Alternatively, Yadav & Thorngren (2017) argued that the surprisingly large radii of hot Jupiters indicate that the stellar deposition of heat into their interiors should enhance convective dynamo activity, leading to inflated interiors and stronger magnetic fields. It is also possible that the dense stellar wind environment in which these hot Jupiters orbit their host stars may preclude the escape of any ECM radio emissions (e.g., Weber et al. (2017); Kavanagh et al. (2019)). Together, these considerations demonstrate that the detection of radio emissions from substellar objects will provide valuable information about myriad system properties and parameters.

Since another focus of our effort was to search for stellar flaring induced by star-planet interactions, we should also consider the frequency ranges that correspond to coronal magnetic fields. While the mean solar photospheric magnetic field has strength of  $B \sim 3\text{-}10$  G, within active regions this field can reach  $B \sim 100$  G, and within sunspot umbrae, field strengths as high as  $B \sim 6$  kG have been measured (Priest 2014). Within the solar corona, magnetic fields as high as  $B \sim 2.5$  kG have been measured above photospheric activity regions. Gyroresonance, gyrosynchrotron, and ECM emissions all contribute to solar coronal radio emissions that range in frequency from  $\nu = 1$  to 20 GHz (Aschwanden 2005). Among these, only activity caused by the latter two processes would be detectable at great distances. Thus, the frequency range of our survey was well-suited for stellar coronal magnetic fields associated with both intrinsic and star-planet induced activity.

However, our survey failed to detect any direct radio emissions from substellar companion auroral activity, or indirect emissions from induced stellar coronal activity at the frequencies surveyed. Thus, in addition to sensitivity, it is likely that most of our observed targets, with the exceptions of HD 114762 Ab, HD 38529c, HD 196252b, and HR 8799 b, c, d, and e were most likely observed at too high of frequencies to detect companion auroral activity. On the other hand, given the frequencies at which solar radio emissions have been detected and the strength of the magnetic fields associated with stellar active regions, the frequencies at which we searched for star-planet induced stellar radio emissions were entirely plausible.

#### 4.2.3. *Observation Durations*

Since our survey searched for companion auroral emission and radio emissions linked to stellar flares that are induced by star-planet interactions, we must consider both contexts when evaluating the temporal coverage of our survey targets. In the first case, companion auroral radio emission generated by the ECM mechanism is beamed into a hollow cone with large opening angles relative to the magnetic field, that is modulated at the rotation period of the object (Zarka 2007). As described in Table 2, all companion-hosting systems were observed for 0.6 to 7.2 ks. We consider exoplanet rotation periods ranging from  $\sim 10$  hrs as is the case for Jupiter and Saturn, to 3-4 d for spin-orbit synchronized, sidereal rotation (Zarka 2007; de Pater & Lissauer 2015). Thus, in the best case scenario of a distant giant exoplanet that has not undergone significant orbital evolution, our observations only cover  $\sim 10\text{-}20\%$  of rotational phase for magnetic activity (e.g.,  $\epsilon$  Tau). The rotational phase coverage of our two brown dwarf targets, HD 38529c and HD 106252b, is probably significantly better. Magnetically active UCDs have a mean rotation period of 1.22 hrs, although their rotation periods range from perhaps as little as 0.288 hrs (WISEPC J112254.73+255021.5; J1122+25) to  $\sim 50$  hrs (SDSS J151643.01+305344.4) (Route 2017a,b). Since HD 38529c and HD

106252b were both observed for 3.6 ks, if they rotate at the mean UCD rotation period, then their rotational phase coverage is likely  $\sim 80\%$ , although given the spread in rotation periods, it could be as low as  $\sim 2\%$ . A similar result applies to the  $\sim$ M5 HD 114762 Ab.

In the second case of star-planet interactions, both host star rotation periods and hot Jupiter orbital periods are of interest (as is their beat period), as it is necessary to untangle the effects of intrinsic stellar activity from activity induced by star-planet interactions. However, hot Jupiter orbital periods are shorter than the rotational periods of their host stars, making the orbital phase coverage the timescale of interest. As described in Section 3.2, the maximum orbital phase coverage for our hot Jupiter targets is listed in Table 5, with  $\Delta\phi_{orb} \leq 0.08$ . Thus, in order to detect star-planet induced activity and untangle its effects from intrinsic stellar activity, we would likely need nearly complete orbital phase coverage over multiple orbits. As ROME I and ROME II have pointed out, even for as well of a studied case as HD 189733, it still remains unclear whether star-planet interactions occur in that system.

In summary, the duration of our observations provide rotational phase coverage of  $\sim 2$  to  $80\%$  for exoplanet or brown dwarf auroral radio emissions and  $\leq 8\%$  orbital phase coverage of hot Jupiters surveyed for star-planet interactions.

#### 4.2.4. Viewing Geometry

Based on an examination of the Solar System planets, we may assume that the magnetic and rotation axes of exoplanet and brown dwarf companions are roughly aligned, and that they are generally aligned with their orbital axes in low-obliquity orbits. Since ECM-induced auroral emissions are beamed into a hollow cone at angles nearly perpendicular to the magnetic axis of the exoplanet or brown dwarf, the optimal viewing angle for these emissions is at high inclination to the orbital axis. In this scenario, transiting and near-transiting systems, such as HD 189733 and the other targets in Table 5, are optimal targets to search for auroral radio emissions. On the other hand, directly-imaged systems, such as the companions of HR 8799, are only likely to yield radio emissions if the exoplanet magnetic axes are significantly tilted with respect to their orbital axes.

Within the context of the search for radio emissions from star-planet interactions, substellar companions may induce enhanced photospheric, chromospheric, and coronal emissions, including radio emissions, either once per orbit due to magnetic effects, or twice per orbit due to tidal effects. While these effects are thought to occur at particular orbital phases, there are otherwise no additional known geometric effects to consider that may influence their detection.

Therefore, while viewing geometry may enhance or hinder the prospects for the detection of radio emissions on a case by case basis, it should not adversely affect the detection of radio emission from every target. We only suspect it is a contributing factor in the failure to detect emissions from systems viewed at low viewing angles with respect to their companions' orbital axes, such as HR 8799 b, c, d, and e.

#### 4.2.5. Significance

Numerous attempts have been made to detect the auroral emissions from exoplanets at radio wavelengths since the work of Yantis et al. (1977). It is beyond the scope of this paper to discuss in detail the merits of these efforts. Instead, we will briefly assess how our survey instrumentation and strategy compare to previous efforts, before examining how this survey, together with surveys of low-mass stars and brown dwarfs, may guide future detection efforts.

Our survey at AO has several distinguishing features relative to previous work. AO provided exquisite sensitivity at short timescales, enabling us to achieve  $3\sigma$  detection limits of  $\sim 1$  mJy in 0.9 s integrations. This compares very favorably with many previous large surveys that achieved detection limits of  $3\sigma \sim 10$  to 100 mJy in  $\sim 1$  ks integrations at, for instance, the Murchison Wide Array (MWA), the Ukrainian T-shaped Radio Telescope second modification (UTR-2), and the Very Large Array (VLA). We also simultaneously observed over a  $\sim 1$  GHz bandpass, as opposed to many earlier efforts that were limited due to existing technology to bandwidths  $\Delta\nu \leq 50$  MHz. Finally, our effort was spectropolarimetric in nature, yielding dynamic spectra in all four Stokes parameters for every target. Earlier efforts often only measured total intensity (Stokes I) from targets, whereas our survey focused on circularly polarized (Stokes V) emission and used linear polarization (Stokes Q and U) as an RFI mitigation strategy. Newer facilities with more recent technology have continued to improve survey characteristics in the same general directions as our survey (e.g., [Turner et al. \(2021\)](#)).

In [Route & Wolszczan \(2016b\)](#), we discussed trends in  $\nu L_\nu$  and  $\nu L_\nu/L_{bol}$  among UCDs, a class of objects that consists of spectral types  $\geq M7$ , including fully-convective low-mass stars of spectral type M, and brown dwarfs of types L, T, and presumably, Y. Although these objects differ in terms of their near infrared and optical spectroscopy, they display similarities in their magnetism as manifest by X-ray, H $\alpha$ , and radio activity (e.g., [McLean et al. \(2012\)](#)). We noted in our earlier work that our detection of flaring radio emission from two late T brown dwarfs, J1047+21 and J1122+25 ([Route & Wolszczan 2016a](#)), helped to pin down how these trends might evolve toward exoplanet-mass substellar objects. Figures 2 and 3 update the plots (Figures 3 and 4; [Route & Wolszczan \(2016b\)](#)) of detected radio emissions from objects near the stellar/substellar boundary that are pertinent to this discussion, and include a side-by-side comparison of efforts to survey UCDs with our current exoplanet survey efforts.

Jupiter's decametric emission is 4-5 orders of magnitude below the UCD flaring radio emission trend line in  $\nu L_\nu$ . Our  $\sim M5$  dwarf HD 114762 Ab detection limit is somewhat high compared to the trend in UCD radio emissions, but acceptable given its earlier spectral type and other similar detections at M7-M9. In [Route & Wolszczan \(2016b\)](#) we mentioned that radio emission ( $\nu L_\nu$ ) either appears to generally remain constant from M7 to T7, or perhaps declines from L2 to T3, followed by a minor rise from T3 to  $\sim$ T6. Yet at some spectral type  $\gtrsim T7$ , greatly reduced flaring and quiescent radio emission from UCDs and giant exoplanets must occur in order for the trend at  $\sim$ T6 to connect with Jovian emissions. Unfortunately, our non-detection of emissions from HD 106252b ( $\sim$ T9) and HD 38529c ( $\sim$ Y0) does not shed any light on this matter. The upper limits on their emissions exceed the UCD trend line and the emissions from J1047+21 and J1122+25 (Figure 2), but are consistent with expectations of their emitted radio power as a fraction of their total luminosity according to the trends in Figure 3.

We can speculate about how radio emission declines precipitously from spectral types  $\gtrsim T7$ , and smoothly connects the activity from J1047+21 and J1122+25 with the Jovian DAM. Compared with this hypothetical trend, our detection limits for even the most massive exoplanets surveyed, such as those of the HR 8799 system and 70 Vir b, are all likely  $\gtrsim 3$  orders of magnitude above the trend line in Figure 2. Similarly, in terms of radio luminosity as a fraction of bolometric luminosity (Figure 3), for the best case scenario for detection, 51 Peg b, our detection limit was still  $\sim 2$  orders of magnitude too large to be successful. Nevertheless, consideration of a hypothetical  $\nu L_\nu$  luminosity trend linking UCD radio activity with that from giant exoplanets suggests that a  $\gtrsim 3$  order-of-magnitude increase

in sensitivity may be required to detect exoplanet emissions. This estimate is somewhat greater than that of Lazio et al. (2004), but consistent with the range suggested by Zarka (2007).

On the other hand, an appraisal of the search for enhanced coronal activity from star-planet interactions is more optimistic. Figure 1 demonstrates that an approximately single order of magnitude increase in sensitivity should make stellar flares of the nearest active stars, such as HD 189733A, accessible. An improvement in sensitivity of  $\sim 10^2$  would also enable the characterization of coronal activity from older, less active stars such as the Sun. However, given the difficulty of untangling star-planet induced flaring from intrinsic coronal activity (i.e. ROME I), searches for this phenomenon will require repeated observations over multiple epochs that occur close together in time.

#### 4.3. Implications for Direct Emissions from Exoplanets within Habitable Zones

Two of our targeted systems host exoplanets (or exomoons) that are within their host stars' HZs for the entire duration of their orbits: HD 10697b and 55 Cnc f. Several others spend a fraction of their orbit within the optimistic HZ, such as HD 38529c (57%), HD 50554b (26%), HD 106252b (20%)<sup>4</sup> (Kane & Gelino 2012; Kopparapu et al. 2014). Both HD 10697b and 55 Cnc f are significantly more massive than the Earth, so that any life within those systems would likely reside on orbiting exomoons. Perhaps such exomoons could generate powerful radio emissions akin to the Io-controlled DAM, and their presence could be inferred through the modulation of exoplanetary radio emissions by the exomoons' orbital periods.

It may be of interest to various communities how our radio survey of exoplanets at AO compares to efforts by SETI that have searched for technosignatures, such as those conducted via Project Phoenix at multiple facilities and more recently, those at the Allen Telescope Array (e.g., Harp et al. (2016)). The exquisitively sensitive Mock Spectrometer at AO could only detect signals as narrow in frequency as 20.9 kHz over a wide bandpass (resampled to 83.6 kHz to improve signal-to-noise characteristics). This compares favorably with remote observations of astrophysical phenomenon, such as the Jovian nKOM radiation, with bandwidths  $\Delta\nu \sim 100$  kHz, but unfavorably with *in situ* measurements of the terrestrial auroral kilometric radiation (AKR) which has instantaneous bandwidths  $\Delta\nu < 1$  kHz (Treumann 2006; de Pater & Lissauer 2015). By comparison, previous searches for technosignatures have required bandwidths of  $\Delta\nu < 1$  Hz to  $\Delta\nu \sim 100$  Hz. Although our principal aims in this study were to search for auroral exoplanetary radio emissions and coronal emissions from star-planet interactions, the results in Table 3 also place upper limits on the detectability of technosignatures within surveyed habitable systems across the bandpass ranging from  $\sim 4255$  to 5330 MHz. Using the narrowest frequency resolution, together with the least and most sensitive observations of our survey, those of the 51 Peg and 55 Cnc systems, respectively, we achieve a  $3\sigma$  threshold signal level of  $43 \times 10^{-26}$  W m<sup>-2</sup> and  $21 \times 10^{-26}$  W m<sup>-2</sup>, respectively.

## 5. CONCLUSION

In 2010-2011, we initiated a survey of exoplanets and brown dwarfs in a quest to detect and characterize their radio emissions, and thereby gain insight into their magnetic activity, magnetic fields, and surrounding plasma environments. The results of the UCD portion of the survey were presented previously (Route & Wolszczan 2012, 2013). In this third installment in the Radio Observations of Magnetized Exoplanets (ROME) series, we take a step back from analyzing the details

<sup>4</sup> “Habitable Zone Gallery,” available at <http://www.hzgallery.org/table.html>

of a particularly interesting exoplanetary system, HD 189733A/B/b (ROME I and II), and present the results of the entire exoplanet portion of the survey conducted at AO. This survey sought two types of radio emission. The first type are those powered by stellar wind interactions with exoplanet magnetospheres, leading to the generation of Jupiter-like auroral radio emissions powered by the electron cyclotron maser (ECM). The second type are those generated by tidal or magnetic star-planet interactions with close-in exoplanets that may induce enhanced coronal, transition region, chromospheric, and photospheric activity in their host stars. Such activity may generate powerful ECM or gyrosynchrotron flares that are phased to the exoplanet orbit.

Our survey leveraged the best technology to date: the exquisitely sensitive 305-m Arecibo radio telescope. With this telescope, we targeted 17 apparently exoplanet-hosting systems, some with multiple exoplanets. We targeted systems with massive exoplanets because their greater mass and reservoir of internal energy may drive more powerful convective dynamos that may generate stronger magnetic fields than generally has been anticipated. Eight of our systems also feature an exoplanet within 0.1 au of its host star to maximize the probability of creating star-planet interactions. Our survey was conducted at 4.2–5.2 GHz, in order to search for stronger magnetic fields and because this frequency range is optimal for the detection of solar radio emissions. We leveraged the Mock Spectrometers to construct dynamic spectra in all four Stokes parameters. Both ECM and gyrosynchrotron activity are characterized by circularly polarized emissions; thus the selection of events based on circular polarization fractions  $\gtrsim 10\%$  also acts as an RFI mitigation strategy. All targets were observed for  $\lesssim 2$  hrs, the maximum amount of time it takes for them to transit the fixed dish.

Our survey did not detect any signatures of exoplanet auroral emissions, or stellar radio flares. Our  $3\sigma$  sensitivity for targeted systems ranged from 0.98–2.1 mJy, resulting in  $\nu L_\nu$  upper limits of  $5.0 \times 10^{23}$  ergs s $^{-1}$  to  $1.5 \times 10^{25}$  ergs s $^{-1}$ . These luminosity detection thresholds correspond to modest ECM flares, such as those that appear on the M3.5 AD Leo, and powerful gyrosynchrotron flares, such as from the K4+K7.5 BY Dra AB system. It has been hypothesized that extremely luminous optical superflares from FGK stars might be caused by star-planet interactions, which have luminosities  $L \sim 5 \times 10^{31}$  ergs s $^{-1}$ . Although our survey was sensitive to radio emissions of equal energy output to these optical superflares, it is unclear whether the *radio* counterparts to such flares would be detectable with current instrumentation.

Several of the targeted systems we surveyed are now known to host low-mass star or brown dwarf companions. These systems include HD 114762 Ab ( $\sim$ M5), HD 106252b ( $\sim$ T9), and HD 38529c ( $\sim$ Y0). Similar objects are known to be powerful radio emitters, especially in the  $\sim$ 5 GHz frequency window, yet no emissions were detected. In each of these cases, the object was likely observed for a significant fraction of its rotation period, suggesting that they are either magnetically inactive, or sporadic radio emitters, as is not uncommon among UCDs (spectral types  $\geq$ M7).

Based on empirically-derived radiometric Bode's laws, several of our targets were thought to be especially promising for the generation of high-frequency radio emissions, including HD 38529c, HD 106252b, 70 Vir b, 55 Cnc d, HD 178911 Bb, HD 10697b, and HD 50554b. However, no signs of auroral radio emissions were detected. Several of our targets, including HD 46375, 70 Vir, 51 Peg, HD 209458 and HD 189733 have previously been investigated for signs of chromospheric activity enhancement that may be due to star-planet interactions. In many of these cases, subsequent work demonstrated that they do not seem to exhibit increased magnetic activity phased with the orbital

or beat periods of their hot Jupiter companions. Similarly, our search for enhanced coronal activity did not reveal any promising signs of activity.

There are several potential reasons for why this search failed. First, if we construct a trend line connecting the radio activity from the coolest, latest type brown dwarfs to that of Jupiter, we find that instrumental sensitivity must increase by  $\gtrsim 10^3$  in order to detect auroral radio emissions. More optimistically, star-planet enhanced coronal activity likely require a  $\gtrsim 10^1$  increase in sensitivity to be detected at radio wavelengths. Second, although it is likely that the frequency range that we observed targets at was too high, it remains unknown what are the cutoff frequencies (local cyclotron frequencies) of giant exoplanets. However, the frequency range with which we searched for enhanced coronal emissions due to star-planet interactions was appropriate. Third, since giant exoplanet rotation periods are likely  $\gtrsim 10$  hrs, our rotational phase coverage of their auroral activity varied from 2–80%. In the search for star-planet interactions, our orbital phase coverage was  $\leq 8\%$  for close-in, hot exoplanet targets.

This diagnosis of our survey points the way to improving the productivity of future searches for exoplanet auroral emissions and enhanced coronal activity due to star-planet interactions. First, great improvements in sensitivity are required to search for both types of emission, although only an increase in sensitivity of  $\sim 10$ –100 is required to enable the search for enhanced coronal activity from star-planet interactions on the nearest stars. For the detection of exoplanet auroral emissions, the situation is rather more pessimistic. Second, future instrumentation should seek to simultaneously observe as wide of a bandpass as possible given the great uncertainty in exoplanet magnetic field strengths, and therefore, the frequency of their cyclotron emissions. Such an advance will also improve the ability to detect flares from star-planet interactions. Third, future surveys should leverage full Stokes parameters to distinguish and characterize among various types of astrophysical emission, and as an RFI mitigation strategy. Fourth, future work will require longer, and more frequent, observations of planet-hosting systems. High cadence observations will enable researchers to untangle the effects of intrinsic stellar activity from differentially rotating stars, from enhanced activity induced by tidal and magnetic star-planet interactions, and from variable and sporadic exoplanet auroral radio emissions.

## 6. ACKNOWLEDGMENTS

MR would like to acknowledge support from the Center for Exoplanets and Habitable Worlds and the Zaccheus Daniel Fellowship. The Center for Exoplanets and Habitable Worlds is supported by the Pennsylvania State University, and the Eberly College of Science. Data storage and analysis support has been made possible with the Theodore Dunham, Jr. Grants for Research in Astronomy. At the time of the observations that are the subject of this publication, the Arecibo Observatory was operated by SRI International under a cooperative agreement with the National Science Foundation (AST-1100968), and in alliance with Ana G. Méndez-Universidad Metropolitana, and the Universities Space Research Association.

This research has made use of NASA’s Astrophysics Data System and the SIMBAD database, operated at CDS, Strasbourg, France. Guidance on properties and publications related to objects of interest were obtained from the catalog located at [exoplanet.eu](http://exoplanet.eu).

*Facility:* Arecibo

*Software:* IDL, MATLAB

## REFERENCES

Aschwanden, M. J. 2005, Physics of the Solar Corona (Chichester, UK: Praxis Publishing Ltd.)

Baines, E. K., McAlister, H. A., Ten Brummelaar, T. A., et al. 2008, *ApJ*, 680, 728

Bakos, G. Á., Knutson, H., Pont, F., et al. 2006, *ApJ*, 650, 1160

Baraffe, I., Chabrier, G., Barman, T. S., Allard, F., & Hauschildt, P. H. 2003, *A&A*, 402, 701

Barrow, C. H., & Morrow, D. P. 1968, *ApJ*, 152, 593

Bastian, T. S., Benz, A. O., & Gary, D. E. 1998, *ARA&A*, 36, 131

Benz, A. O., & Güdel, M. 2010, *ARA&A*, 48, 241

Boisse, I., Moutou, C., Vidal-Madjar, A., et al. 2009, *A&A*, 495, 959

Bouchy, F., Udry, S., Mayor, M., et al. 2005, *A&A*, 444, L15

Bourrier, V., Dumusque, X., Dorn, C., et al. 2018, *A&A*, 619, A1

Bourrier, V., Wheatley, P. J., Lecavelier des Etangs, A. 2020, *MNRAS*, 493, 559

Brandt, G. M., Brandt, T. D., Dupuy, T. J., Michalik, D., & Marleau, G.-D. 2021, *ApJL*, 915, L16

Burgasser, A. J., Melis, C., Todd, J., et al. 2015, *AJ*, 150, 180

Burke, B. F., & Franklin, K. L. 1955, *J. Geophys. Res.*, 60, 213

Butler, R. P., Vogt, S. S., Marcy, G. W., et al. 2004, *ApJ*, 617, 580

Butler, R. P., Wright, J. T., Marcy, G. W., et al. 2006, *ApJ*, 646, 505

Canto Martins, B. L., das Chagas, M. L., Alves, S., et al. 2011, *A&A*, 530, A73

Chabrier, G. & Baraffe, I. 2000, *ARA&A*, 38, 337

Chabrier, G., Baraffe, I., Leconte, J., Gallardo, J., & Barman, T. 2009, AIP Conference Proceedings 1094, 102

Charbonneau, D., Brown, T. M., Latham, D. W., & Mayor, M. 2000, *ApJ*, 529, L45

Christensen, U. R. 2010, *SSRv*, 152, 565

Christensen, U. R., Holzwarth, V., & Reiners, A. 2009, *Nature*, 457, 167

Crida, A., Ligi, R., Dorn, C., Borsa, F., & Lebreton, Y. 2018, *RNAAS*, 2, 3

Cuntz, M., Saar, S. H., & Musielak, Z. E. 2000, *ApJ*, 533, L151

Cuntz, M., & Shkolnik, E. 2002, *AN*, 323, 387

Cushing, M. C., Kirkpatrick, J. D., Gelino, C. R., Griffith, R. L., Skrutskie, M. F., et al. 2011, *ApJ*, 743, 50

Dawson, R. I., & Johnson, J. A. 2018, *ARA&A*, 56, 175

de Pater, I., & Lissauer, J. J. 2015, *Planetary Sciences* (Updated 2nd ed.; Cambridge, UK: Cambridge University Press)

Demory, B.-O., Gillon, M., de Wit, J., et al. 2016, *Nature*, 532, 207

Dulk, G. A. 1987, in *Cool Stars, Stellar Systems, and the Sun*, Fifth Cambridge Workshop, ed. J. L. Linsky & R. E. Stencel (Berlin: Springer), 72

Fares, R., Donati, J.-F., Moutou, C., et al. 2010, *MNRAS*, 406, 409

Fares, R., Bourrier, V., Vidotto, A. A., Moutou, C., Jardine, M. M., et al. 2017, *MNRAS*, 471, 1246

Fischer, D. A., & Valenti, J. 2005, *ApJ*, 622, 1102

Fischer, D. A., Marcy, G. W., Butler, R. P., Vogt, S. S., & Apps, K. 1999, *PASP*, 111, 755

Fischer, D. A., Marcy, G. W., Butler, R. P., et al. 2001, *ApJ*, 551, 1107

Fischer, D. A., Marcy, G. W., Butler, R. P., et al. 2003, *ApJ*, 586, 1394

Fischer, D. A., Marcy, G. W., Butler, R. P., et al. 2008, *ApJ*, 675, 790

Forveille, T., Bonfils, X., Delfosse, X., et al. 2009, *A&A*, 493, 645

Fritz Benedict, G., McArthur, B. E., Bean, J. L. 2010, *AJ*, 139, 1844

Gaia Collaboration, 2018, *A&A*, 616, A1

Ge, J., van Eyken, J., Mahadevan, S., et al. 2006, *ApJ*, 684, 683

Griessmeier, J.-M., Zarka, P., & Spreeuw, H. 2007, *A&A*, 475, 359

Güdel, M., Audard, M., Kashyap, V. L., Drake, J. J., & Guinan, E. F. 2003, *ApJ*, 582, 423

Guillot, T. 2005, *Annu. Rev. Earth Planet. Sci.*, 33, 495

Guilluy, G., Sozzetti, A., Brogi, M., et al. 2019, *A&A*, 625, A107

Harp, G. R., Richards, J., Tarter, J. C., Drehler, J., Jordan, J., et al. 2016, *AJ*, 152, 181

Henry, G. W., Marcy, G. W., Butler, R. P., & Vogt, S. S. 2000, *ApJ*, 529, L41

Ignace, R., Giroux, M. L., & Luttermoser, D. G. 2010, MNRAS, 402, 2609

Jensen, A. G., Redfield, S., Endl, M., et al. 2012, ApJ, 751, 86

Kane, S. R., & Gelino, D. M. 2012, PASP, 124, 914

Kane, S. R., Boyajian, T. S., Henry, G. W., et al. 2015, ApJ, 806, 60

Kao, M. M., Hallinan, G., Pineda, J. S., Stevenson, D., & Burgasser, A. 2018, ApJS, 237, 25

Kavanagh, R. D., Vidotto, A. A., Fionnagáin, D. Ó., et al. 201, MNRAS, 485, 4529

Kiefer, F., Hébrard, G., Lecavelier des Etangs, A., et al. 2021, A&A, 645, A7

Kopparapu, R. K., Ramirez, R. M., SchottelKotte, J., et al. 2014, ApJL, 787, L29

Kunitomo, M., Ikoma, M., Sato, B., Katsuta, Y., & Ida, S. 2011, ApJ, 737, 66

Knutson, H. A., Charbonneau, D., Allen, L. E., et al. 2007, Nature, 447, 183

Latham, D. W., Mazeh, T., Stefanik, R. P., Mayor, M., & Burki, G. 1989, Nature, 339, 38

Lazio, T. J. W., Farrell, W. M., Dietrick, J., et al. 2004, ApJ, 612, 511

Lazio, T. J. W. 2018, in *Handbook of Exoplanets*, eds. H. J. Deeg & J. A. Belmonte (Springer International Publishing AG), 38

Luhn, J. K., Bastien, F. A., Wright, J. T., et al. 2019, AJ, 157, 149

Lyutikov, M., Barkov, M., Route, M., et al. 2020, (arXiv:2004.11474v1)

Marcy, G. W. & Butler, R. P. 1996, ApJ, 464, L147

Marcy, G. W., Butler, R. P., & Vogt, S. S. 2000, ApJ, 536, L43

Marcy, G. W., Butler, R. P., Williams, E., et al. 1997, ApJ, 481, 926

Marois, C., Zuckerman, B., Konopacky, Q. M., Macintosh, B., & Barman, T. 2010, Nature, 468, 1080

Martins, J. H. C., Santos, N. C., Figueira, P., et al. 2015, A&A, 576, A134

Mayor, M. & Queloz, D. 1995, Nature, 378, 355

McLean, M., Berger, E., & Reiners, A. 2012, ApJ, 746, 23

Nichols, J. D. 2012, MNRAS, 427, L75

Nielsen, E. L., De Rosa, R. J., McIntosh, B., et al. 2019, AJ, 158, 13

Oppenheimer, B. R., Baranec, C., Beichman, C., et al. 2013, ApJ, 768, 24

Perrier, C., Sivan, J.-P., Naef, D., et al. 2003, A&A, 410, 1039

Pick, M., & Vilmer, N. 2008, A&A Rv, 16, 1

Priest, E. 2014, *Magnetohydrodynamics of the Sun* (Cambridge, UK: Cambridge University Press)

Reffert, S., & Quirrenbach, A. 2011, A&A, 527, A140

Reid, I. N., & Hawley, S. L. 2005, *New Light on Dark Stars* (2nd ed.; Chichester, UK: Springer-Praxis Books)

Reiners, A., & Christensen, U. R. 2010, A&A, 522, A13

Richey-Yowell, T., Kao, M. M., Pineda, J. S., Shkolnik, E. L., & Hallinan, G. 2020, ApJ, 903, 74

Route, M. 2013, PhD Dissertation, Pennsylvania State University

Route, M. 2017a, ApJ, 843, 115

Route, M. 2017b, ApJ, 845, 66

Route, M. 2019, ApJ, 872, 79

Route, M., & Looney, L. W. 2019, ApJ, 887, 229

Route, M. & Wolszczan, A. 2012, ApJL, 747, L22

Route, M. & Wolszczan, A. 2013, ApJ, 773, 18

Route, M. & Wolszczan, A. 2016a, ApJL, 821, L21

Route, M. & Wolszczan, A. 2016b, ApJ, 830, 85

Rubenstein, E. P., & Schaefer, B. E. 2000, ApJ, 529, 1031

Saar, S. H., & Cuntz, M. 2001, MNRAS, 325, 55

Salter, C. 2009, *An Astronomer's Guide to the Arecibo 305-m Telescope* (Arecibo, PR: National Astronomy and Ionosphere Center)

Sánchez-Lavega, A. 2004, ApJ, 609, L87

Sato, B., Izumiura, H., Toyota, E., et al. 2007, ApJ, 661, 527

Schaefer, B. E., King, J. R., & Deliyannis, C. P. 2000, ApJ, 529, 1026

Seager, S., Kuchner, M., Hier-Majumder, C. A., & Militzer, B. 2007, ApJ, 669, 1279

Shkolnik, E., Walker, G. A. H., & Bohlender, D. A. 2003, ApJ, 597, 1092

Shkolnik, E., Walker, G. A. H., Bohlender, D. A., Gu, P.-G., Kürster, M. 2005, ApJ, 622, 1075

Shkolnik, E., Bohlender, D. A., Walker, G. A. H., & Collier Cameron, A. 2008, ApJ, 676, 628

Simpson, E. K., Baliunas, S. L., Henry, G. W., & Watson, C. A. 2010, MNRAS, 408, 1666

Sirothia, S. K., Lecavelier des Etangs, A., Gopal-Krishna, Kantharia, N. G., & Ishwar-Chandra, C. H. 2014, *A&A*, 562, A108

Southworth, J. 2010, *MNRAS*, 408, 1689

Stepanov, A. V., Kliem, B., Zaitsev, V. V., et al. 2001, *A&A*, 372, 1072

Treumann, R. A. 2006, *A&A Rv*, 13, 229

Trigilio, C., Leto, P., Umana, G., Buemi, C. S., & Leone, F. 2011, *ApJL*, 739, L10

Turner, J. D., Zarka, P., Griesmeier, J.-M., et al. 2021, *A&A*, 645, A59

Vogt, S. S., Marcy, G. M., Butler, R. P., & Apps, K. 2000, *ApJ*, 536, 902

von Braun, K., Boyajian, T. S., Ten Brummelaar, T. A., et al. 2011, *ApJ*, 740, 49

von Braun, K., Boyajian, T. S., van Belle, G. T., et al. 2014, *MNRAS*, 438, 2413

Wang, J., & Ford, E. B. 2011, *MNRAS*, 418, 1822

Weber, C., Lammer, H., Shaikhislamov, I. F., et al. 2017, *MNRAS*, 469, 3505

Williams, P. K. G., & Berger, E. 2015, *ApJ*, 808, 189

Williams, P. K. G., Cook, B. A., & Berger, E. 2014, *ApJ*, 785, 9

Williams, P. K. G., Berger, E., Irwin, J., Berta-Thompson, Z. K., & Charbonneau, D. 2015, *ApJ*, 799, 192

Williams, P. K. G., Gizis, J. E., & Berger, E. 2017, *ApJ*, 834, 117

Wittenmyer, R. A., Endl, M., Cochran, W. D. 2009, *ApJS*, 182, 97

Yadav, R. K., & Thorngren, D. P. 2017, *ApJL*, 849, L12

Yantis, W. F., Sullivan, W. T., III, & Erickson, W. C. 1977, *BAAS*, 9, 453

Zaghou, M., & Collins, G. W. 2018, *ApJ*, 862, 19

Zarka, P. 1998, *J. Geophys. Res.*, 103, 20,159

Zarka, P., Cecconi, B., & Kurth, W. S. 2004, *J. Geophys. Res.*, 109, A09S15

Zarka, P. 2007, *Planet. Space Sci.*, 55, 598

Zic, A., Lynch, C., Murphy, T., Kaplan, D. L., & Chandra, P. 2019, *MNRAS*, 483, 614

Zucker, S., Naef, D., Latham, D. W., et al. 2002, *ApJ*, 568, 363

**Table 1.** Survey Target Properties

Name	R.A. (hh mm ss)	Dec. ( ° ' '')	Host Star	Dist. (pc)	Semimajor Axis (AU)	Period (d)	Mass (M <sub>J</sub> )	Discovery Ref(s)	Properties Refs
HD 10697 b <sup>a</sup>	01 44 55	+20 04 59	G5 IV	32.6	2.12	1072.3	6.837	1	<u>1,2</u>
ε Tau b <sup>b</sup>	04 28 37	+19 10 50	K0 III	47.5	1.90	594.9	7.34	3	<u>3,4,4</u>
GJ 176 b <sup>c</sup>	04 42 56	+18 57 29	M2.5 Ve	9.4	0.066	8.7836	0.0264	5	<u>5,5</u>
HD 38529 b	05 46 34	+01 10 05	G4 IV	42.4	0.131	14.31	0.90	6	<u>6,7,7</u>
	c				3.697	1236.14	17.6 <sup>d</sup>	8	<u>6,7,7</u>
HD 46375 b	06 33 12	+05 27 46	K1 IV	33.4	0.0398	3.024	0.226	9	<u>10,10</u>
HD 50554 b	06 54 42	+24 14 44	F8 V	31.03	2.28	1224	4.46	11	<u>10,10</u>
55 Cnc e	08 52 37	+28 20 02	K0 V	12.59	0.0154	0.7365	0.027	12	<u>13,14,13</u>
	b				0.1134	14.6516	0.8036	12	<u>13,14,14</u>
	c				0.2373	44.3989	0.1611	12	<u>13,14,14</u>
	f				0.7708	259.88	0.1503	12	<u>13,14,14</u>
	d				5.450	5574.2	3.12	12	<u>13,14,14</u>
GJ 436 b	11 42 11	+26 42 23	M2.5 V	10.23	0.02887	2.644	0.0737	15	<u>10,16,16</u>
HD 102195 b	11 45 42	+02 49 17	G8 V	29	0.049	4.114	0.46	17	<u>17,18,18</u>
HD 106252 b	12 13 29	+10 02 29	G0 V	37.4	2.6	1531	30.6 <sup>e</sup>	11	<u>10,19,19</u>
HD 114762 Ab	13 12 19	+17 31 01	F9 V	38.7	0.361	83.915	147 <sup>f</sup>	20	<u>20,21,21</u>
70 Vir b	13 28 26	+13 47 12	G4 V	22	0.481	116.69	7.4	22	<u>22,23,23</u>
HD 178911 Bb	19 09 03	+34 35 59	G5	46.73	0.339	71.484	7.03	24	<u>25,25</u>
HD 189733 b	20 00 43	+22 42 39	K2 V	19.78	0.0313	2.219	1.13	26	<u>27,26,28</u>
HD 195019 b	20 28 17	+18 46 12	G3 IV/V	37.4	0.1388	18.2	3.69	29	<u>10,10</u>
HD 209458 b	22 03 10	+18 53 04	G0 V	47	0.0467	3.5247	0.714	30,31	<u>30,31,16,16</u>
51 Peg b	22 57 27	+20 46 07	G2 IV	15.36	0.053	4.231	0.46	32	<u>10,33</u>

NOTE—Exoplanet, brown dwarf, and low-mass stellar companion hosting system properties. In the properties references column (column 10), **bold**, underlined, and *italicized* numerals denote distance from Earth, semimajor axis, and orbital period references, respectively. The final number in the column in normal font provides the companion object’s mass reference(s). **References.** (1) [Vogt et al. \(2000\)](#); (2) [Simpson et al. \(2010\)](#); (3) [Sato et al. \(2007\)](#); (4) [Kunitomo et al. \(2011\)](#); (5) [Forveille et al. \(2009\)](#); (6) [Fischer et al. \(2001\)](#); (7) [Fritz Benedict et al. \(2010\)](#); (8) [Fischer et al. \(2003\)](#); (9) [Marcy et al. \(2000\)](#); (10) [Butler et al. \(2006\)](#); (11) [Perrier et al. \(2003\)](#); (12) [Fischer et al. \(2008\)](#); (13) [Crida et al. \(2018\)](#); (14) [Bourrier et al. \(2018\)](#); (15) [Butler et al. \(2004\)](#); (16) [Southworth \(2010\)](#); (17) [Ge et al. \(2006\)](#); (18) [Guilluy et al. \(2019\)](#); (19) [Reffert & Quirrenbach \(2011\)](#); (20) [Latham et al. \(1989\)](#); (21) [Kiefer et al. \(2021\)](#); (22) [Marcy & Butler \(1996\)](#); (23) [Kane et al. \(2015\)](#); (24) [Zucker et al. \(2002\)](#); (25) [Wittenmyer et al. \(2009\)](#); (26) [Bouchy et al. \(2005\)](#); (27) [Gaia Collaboration \(2018\)](#); (28) [Boisse et al. \(2009\)](#); (29) [Fischer et al. \(1999\)](#); (30) [Henry et al. \(2000\)](#); (31) [Charbonneau et al. \(2000\)](#); (32) [Mayor & Queloz \(1995\)](#); (33) [Martins et al. \(2015\)](#).

<sup>a</sup>Also known as 109 Psc b.

<sup>b</sup>Also known as HD 28305 b.

<sup>c</sup>Also known as HD 285968 b.

<sup>d</sup>With a mass of  $0.017M_{\odot}$ , 5 Gyr isochrones yield  $T_{eff} \sim 430$  K and an estimated spectral type of Y0 ([Baraffe et al. 2003; Cushing et al. 2011](#)).

<sup>e</sup>5 Gyr isochrones yield  $T_{eff} \sim 610$  K and an estimated spectral type of T9 for an object of mass  $0.029M_{\odot}$  ([Baraffe et al. 2003; Cushing et al. 2011](#)).

<sup>f</sup>Figure 10 in [Chabrier & Baraffe \(2000\)](#) indicates spectral type M5 roughly corresponds to a  $0.140M_{\odot}$  object that is 5 Gyr old of solar metallicity.

**Table 2.** Observations List

Name	UT Date	File Date	Scan Range	Number	Time on
	(yyyyymmdd)	(yyyyymmdd)		of Scans	Source (ks)
HD 10697	2010 12 21	2010 12 20	00000-01200	4	2.4
	ε Tau	2010 01 09	00000-02000	7	4.2
	2010 12 18	2010 12 17	10100-10700*	3	1.8
	2010 12 18	2010 12 18	00000-00400	1	0.6
GJ 176	2010 12 21	2010 12 20	02500-03600	4	2.4
	2010 01 10	2010 01 09	01800-03500	6	3.6
	2010 12 19	2010 12 18	12500-13100*	3	1.8
	2010 12 19	2010 12 19	00000-00700	2	1.2
HD 38529	2010 01 09	2010 01 08	02100-03800	6	3.6
HD 46375	2010 01 10	2010 01 09	03600-04800*	5	3.0
	2010 01 10	2010 01 10	00000-00400	1	0.6
HD 50554	2010 01 09	2010 01 08	03900-04200*	2	1.2
	2010 01 09	2010 01 09	00000-00400	1	0.6
	2010 12 18	2010 12 18	00500-02800	8	4.8
	2010 12 19	2010 12 19	00800-01900	4	2.4
55 Cnc	2011 01 02	2011 01 02	02700-05000	8	4.8
GJ 436	2010 01 06	2010 01 06	01800-03500	6	3.6
HD 102195	2010 01 07	2010 01 07	00000-01700	6	3.6
HD 106252	2010 01 07	2010 01 07	01800-03500	6	3.6
HD 114762	2010 01 07	2010 01 07	03600-03800	1	0.6
	2011 01 02	2011 01 02	08700-10500	7	4.2
70 Vir	2010 01 06	2010 01 06	03600-05600	7	4.2
HD 178911 B	2011 07 20	2011 07 19	06200-07100*	4	2.4
	2011 07 20	2011 07 20	00000-01000	3	1.8
HD 189733	2011 09 07	2011 09 06	00000-03500	12	7.2
HD 195019	2011 07 20	2011 07 20	01100-04000	10	6.0
HD 209458	2011 07 20	2011 07 20	04100-05800	6	3.6
	2011 09 07	2011 09 06	03600-05500	7	4.2
51 Peg	2011 07 19	2011 07 18	04100-06100	7	4.2
	2011 09 07	2011 09 06	05700	1	0.6
	2011 09 07	2011 09 07	00000-01600	5	3.0

NOTE—Asterisks in the scan range column denote an observing session that directly continued onto the following day.

**Table 3.** Survey Detection Results

Object	Mass	Detected Flux	$\nu L_\nu$	$\nu L_\nu$	$\nu L_\nu a$	$L_{bol}$	$\nu L_\nu / L_{bol}$
	(M <sub>J</sub> )	(mJy)	(ergs s <sup>-1</sup> )	(log L <sub>⊙</sub> )	(log L <sub>J,rad</sub> )	(log L <sub>⊙</sub> )	(log L <sub>⊙</sub> )
HD 10697 b	6.837	<1.305	<7.413×10 <sup>24</sup>	<-8.714	<6.956	-7.293	<-1.421
ε Tau b	7.34	<1.101	<1.382×10 <sup>25</sup>	<-8.461	<7.209	-6.010	<-2.451
GJ 176 b	0.0264	<1.065	<5.030×10 <sup>23</sup>	<-9.883	<5.788	-8.039	<-1.844
HD 38529 b	0.90	<1.425	<1.369×10 <sup>25</sup>	<-8.448	<7.223	-6.934	<-1.514
c	17.6	<1.425	<1.369×10 <sup>25</sup>	<-8.448	<7.223	-3.117	<-5.331
HD 46375 b	0.226	<1.134	<6.761×10 <sup>24</sup>	<-8.754	<6.916	-4.441	<-4.313
HD 50554 b	4.46	<1.038	<5.342×10 <sup>24</sup>	<-8.857	<6.814	-8.000	<-0.857
55 Cnc e	0.027	<0.984	<8.336×10 <sup>23</sup>	<-9.663	<6.007	-5.307	<-4.356
b	0.8036	<0.984	<8.336×10 <sup>23</sup>	<-9.663	<6.007	-7.741	<-1.922
c	0.1611	<0.984	<8.336×10 <sup>23</sup>	<-9.663	<6.007	-7.278	<-2.385
f	0.1503	<0.984	<8.336×10 <sup>23</sup>	<-9.663	<6.007	-7.998	<-1.665
d	3.12	<0.984	<8.336×10 <sup>23</sup>	<-9.663	<6.007	-9.172	<-0.491
GJ 436 b	0.0737	<1.047	<5.856×10 <sup>23</sup>	<-9.817	<5.854	-6.616	<-3.201
HD 102195 b	0.46	<1.302	<5.852×10 <sup>24</sup>	<-8.817	<6.854	-7.178	<-1.639
HD 106252 b	30.6	<1.194	<8.926×10 <sup>24</sup>	<-8.634	<7.037	-3.068	<-5.566
HD 114762 Ab	147	<1.140	<9.125×10 <sup>24</sup>	<-8.624	<7.046	-2.750	<-5.874
70 Vir b	7.4	<1.047	<2.708×10 <sup>24</sup>	<-9.152	<6.519	-6.333	<-2.819
HD 178911 Bb	7.03	<1.287	<1.502×10 <sup>25</sup>	<-8.408	<7.263	-6.410	<-1.998
HD 189733 b <sup>b</sup>	1.13	<1.158	<2.421×10 <sup>24</sup>	<-9.200	<6.470	-4.763	<-4.437
HD 195019 b	3.69	<1.203	<8.944×10 <sup>24</sup>	<-8.630	<7.040	-5.422	<-3.208
HD 209458 b	0.714	<1.155	<1.364×10 <sup>25</sup>	<-8.450	<7.221	-4.106	<-4.344
51 Peg b	0.46	<2.067	<2.606×10 <sup>24</sup>	<-9.168	<6.502	-4.097	<-5.071
HR 8799 <sup>c</sup> e	9.6	<1.044	<8.662×10 <sup>24</sup>	<-8.647	<7.024	-4.520	<-4.127
d	7.2	<1.044	<8.662×10 <sup>24</sup>	<-8.647	<7.024	-4.7	<-3.947
c	7.2	<1.044	<8.662×10 <sup>24</sup>	<-8.647	<7.024	-4.7	<-3.947
b	5.8	<1.044	<8.662×10 <sup>24</sup>	<-8.647	<7.024	-5.1	<-3.547

NOTE—Detection limits and radio luminosities of target systems.

<sup>a</sup>Luminosity in terms of the average power output of Jupiter's ECM-induced DAM during maximum solar activity (as opposed to average power or peak power), or  $L_{J,rad} = 8.2 \times 10^{17}$  erg s<sup>-1</sup> (Zarka et al. 2004).

<sup>b</sup>Radio emission flux density upper limit presented in Route (2019), with luminosity updated due to revised distance to HD 189733 (Gaia Collaboration 2018).

<sup>c</sup>Radio emission flux density upper limits for all HR 8799 exoplanets were reported in relation to our first UCD survey (Route & Wolszczan 2013).

**Table 4.** Companion Bolometric Luminosities

Companion	Radius	$T_{eff}$	$L_{bol}$	Refs	Stellar Radius	Stellar $T_{eff}$	Stellar Refs
	( $R_J$ )	(K)	(ergs $s^{-1}$ )		( $R_\odot$ )	(K)	
HD 10697 b	1.152*	255†	$1.954 \times 10^{26}*$	<b>1,2</b>	-	-	-
$\epsilon$ Tau b	1.012*	570*	$3.754 \times 10^{27}*$	<b>3</b>	13.7	4901	<b>4</b>
GJ 176 b	0.183*	417*	$3.507 \times 10^{25}*$	<b>5</b>	0.453	3679	<b>6</b>
HD 38529 b	0.100*	1064*	$4.470 \times 10^{26}*$	<b>3</b>	2.44	5697	<b>7</b>
c	0.955*	3100*	$2.933 \times 10^{30}*$	<b>3,8</b>	-	-	-
HD 46375 b	1.020	1400*	$1.392 \times 10^{29}*$	<b>9,10</b>	-	-	-
HD 50554 b	1.035*	179*	$3.839 \times 10^{25}*$	<b>3</b>	1.11	5929	<b>11, 12</b>
55 Cnc e	0.178	2037†	$1.892 \times 10^{28}*$	<b>13,14</b>	-	-	-
b	0.102*	661*	$6.972 \times 10^{25}*$	<b>3</b>	0.98	5196	<b>13,15</b>
c	0.365*	457*	$2.025 \times 10^{26}*$	<b>5</b>	0.98	5196	<b>13,15</b>
f	0.365*	302*	$3.858 \times 10^{25}*$	<b>5,2</b>	-	-	-
d	1.035*	95*	$2.585 \times 10^{24}*$	<b>3</b>	0.98	5196	<b>13,15</b>
GJ 436 b	0.365	669*	$9.293 \times 10^{26}$	<b>16</b>	-	-	-
HD 102195 b	0.096*	947*	$2.551 \times 10^{26}*$	<b>3</b>	0.837	5291	<b>17</b>
HD 106252 b	0.891*	3300*	$3.281 \times 10^{30}*$	<b>3,8</b>	-	-	-
HD 114762 Ab	-	-	$6.827 \times 10^{30}*$	<b>18</b>	-	-	-
70 Vir b	1.012	473*	$1.784 \times 10^{27}*$	<b>3</b>	1.94	5439	<b>19</b>
HD 178911 Bb	1.023*	450*	$1.495 \times 10^{27}*$	<b>3</b>	1.14	5668	<b>20,21</b>
HD 189733 b	1.154	1093†	$6.619 \times 10^{28}$	<b>22,23</b>	-	-	-
HD 195019 b	1.035*	790*	$1.454 \times 10^{28}*$	<b>3</b>	1.38	5788	<b>20,12</b>
HD 209458 b	1.380	1459*	$3.005 \times 10^{29}$	<b>16</b>	-	-	-
51 Peg b	1.9	1250*	$3.069 \times 10^{29}*$	<b>24,25</b>	-	-	-
HR 8799 e	-	-	$1.159 \times 10^{29}$	<b>26</b>	-	-	-
d	-	-	$7.660 \times 10^{28}$	<b>27</b>	-	-	-
c	-	-	$7.660 \times 10^{28}$	<b>27</b>	-	-	-
b	-	-	$3.049 \times 10^{28}$	<b>27</b>	-	-	-

NOTE—Measured and inferred bolometric luminosities of the surveyed companion low-mass stars, brown dwarfs, and exoplanets. For companion properties (columns 2-4), **bold**, underlined, and *italicized* numerals denote radius, temperature, and luminosity references (column 5), respectively. Similarly, for stellar properties (columns 6-7), **bold** and underlined numerals denote radius and temperature references, respectively, while relevant semi-major axes can be found in Table 1. Asterisks (\*) denote values that are either estimated within the given references, or computed based upon the relevant stellar and orbital properties (see text for more details). Dagger symbols (†) denote companion  $T_{eff}$ s computed by averaging measured minimum and maximum temperatures. Below the horizontal bar are the measured luminosities of the hot, young exoplanets of the HR 8799 system for comparison.

**References.** (1) Luhn et al. (2019); (2) Kane & Gelino (2012); (3) Chabrier et al. (2009); (4) Sato et al. (2007); (5) Seager et al. (2007); (6) von Braun et al. (2014); (7) Fritz Benedict et al. (2010); (8) Chabrier & Baraffe (2000); (9) Wang & Ford (2011); (10) Marcy et al. (2000); (11) Baines et al. (2008); (12) Butler et al. (2006); (13) Crida et al. (2018); (14) Demory et al. (2016); (15) von Braun et al. (2011); (16) Southworth (2010); (17) Guilluy et al. (2019); (18) Reid & Hawley (2005); (19) Kane et al. (2015); (20) Fischer & Valenti (2005); (21) Wittenmyer et al. (2009); (22) Bakos et al. (2006); (23) Knutson et al. (2007); (24) Martins et al. (2015); (25) Marcy et al. (1997); (26) Brandt et al. (2021); (27) Marois et al. (2010).

**Table 5.** Orbital Phase Coverage of Radio Observations

Object	Period	$T_t$ (d)	$a$ (d)	Obs Start (d)		Obs End (d)	Orbital Phases	Orbital Refs
				Monitored				
GJ 176 b	8.7836	54399.790*	55206.590	55206.634	0.853-0.858	55549.655	0.910-0.915	<b>1</b>
HD 46375 b	3.023573	51071.357†	55206.639	55206.683	0.681-0.695	55563.752	0.207-0.287	<b>2</b>
55 Cnc e	0.7365474	57063.210*	55563.752	55563.810	0.789-0.806	55202.865	4.2	<b>3</b>
GJ 436 b	2.64389524	51549.560	55202.865	55202.909	0.849-0.859	53731.701†	55203.898	5.2
HD 102195 b	4.1139	53629.389	55811.509	55811.598	0.568-0.608	52854.830	55762.785	6.7
HD 189733 b <sup>b</sup>	2.218575	53629.389	55811.605	55811.660	0.011-0.023	55762.829	0.861-0.877	4.2
HD 209458 b	3.52474859	52854.830	55761.784	55761.835	0.425-0.438	55811.665	55811.709	2
51 Peg b	4.230785	50001.886†	55761.784	55761.835	0.215-0.226	55811.665	55811.709	0.215-0.226

NOTE—Orbital phase coverage of the AO radio observations for systems with exoplanet targets that have orbital periods  $<10$  d. Orbital periods are reported to maximum precision in the reference. In the orbital references column, **bold** and underlined text denote orbital period and transit time ( $T_t$ ) references, respectively. Transit times, observation start, and observation end dates (columns 3-5) are reported in HJD (or BJD) -2,400,000.

**References.** (1) Forveille et al. (2009); (2) Butler et al. (2006); (3) Bourrier et al. (2018); (4) Southworth (2010); (5) Guilluy et al. (2019); (6) Bouchy et al. (2005); (7) Fares et al. (2017).

<sup>a</sup> $T_t$ s are measured or estimated (†), depending upon the reference. Asterisks (\*) denote values that are in BJD.

<sup>b</sup> Orbital phase coverage from Route (2019).

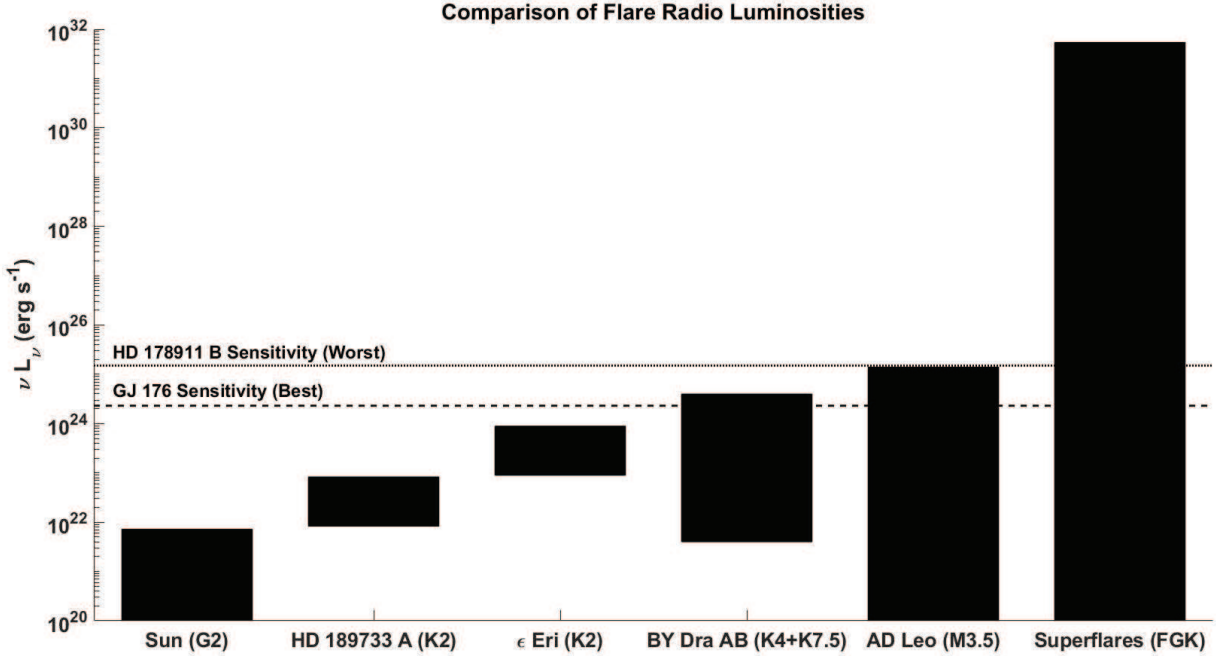


**Figure 1.** Survey  $\nu L_\nu$  radio luminosity upper limits compared to other stellar flare luminosities. For each object, the spectral type(s) are given in parentheses. The flare radio luminosity ranges for HD 189733A,  $\epsilon$  Eri, and the interacting binary BY Dra AB are calculated from their X-ray flare luminosity ranges via the Güdel-Benz relationship (Benz & Güdel 2010; Route 2019). While these emissions are generated by incoherent, gyrosynchrotron flaring, flares observed at AD Leo are created by the ECM process, and due to their coherence and beaming, are more readily detectable (Stepanov et al. 2001). We establish a maximum luminosity for the “Superflares” category using the 15-day  $B$  and  $V$  band flare observations of the F8 IV star 5 Serpentis, although it is non-trivial to relate the optical properties of flares to those at radio wavelengths (Schaefer et al. 2000; Priest 2014). The dashed and dotted lines mark the detection thresholds of our most and least sensitive observations, those at GJ 176 and HD 178911B, respectively, relative to these flare energies.

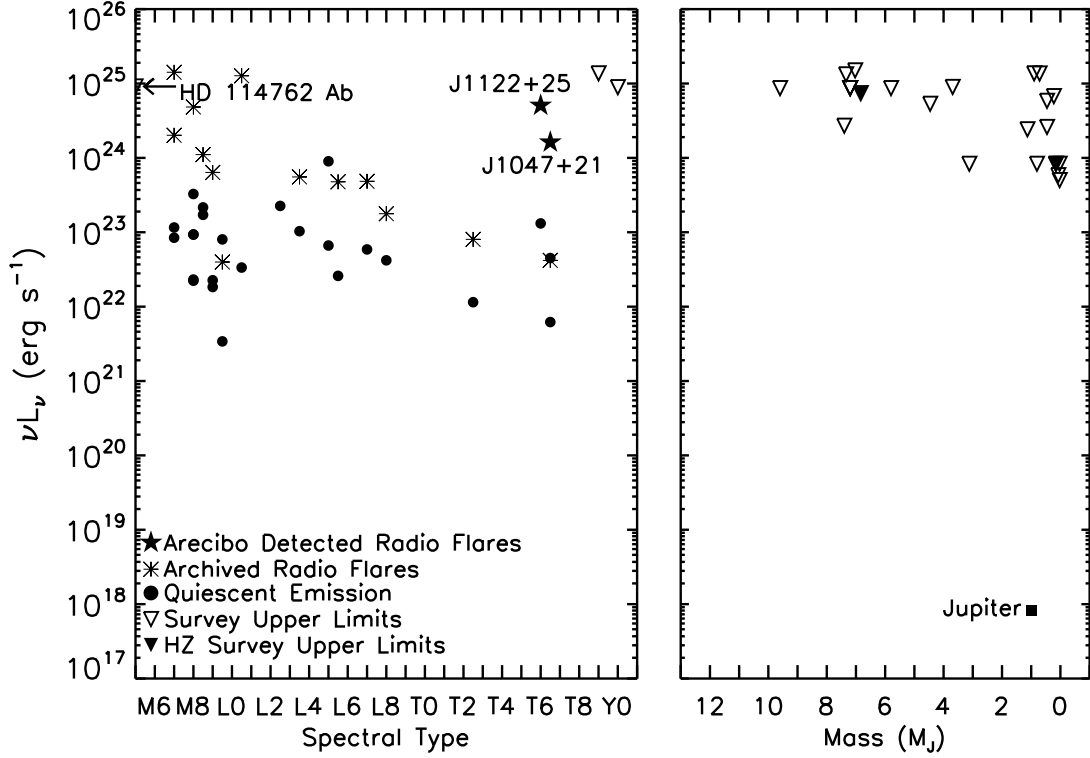


**Figure 2.** Logarithmic plots of  $\nu L_\nu$  radio luminosity upper limits versus spectral type (left panel) or exoplanet mass (right panel) of surveyed brown dwarf and low-mass stellar companions, as compared to previously detected radio-emitting UCDs (Burgasser et al. 2015; Route & Wolszczan 2016b; Route 2017a; Williams & Berger 2015; Williams et al. 2014, 2015, 2017; Zic et al. 2019; Richey-Yowell et al. 2020). The two AO discoveries of the coolest known radio-flaring brown dwarfs near the brown dwarf/ exoplanet boundary are marked by filled stars (Route & Wolszczan 2012, 2016a). HD 114762 Ab appears at upper left with an estimated spectral type of M5. HD 106252b ( $\sim$ T9) and HD 38529c ( $\sim$ Y0) appear in the left panel at upper right. Our earlier upper limits to the radio emission from the four young exoplanets of the HR 8799 system are graphed based on their estimated masses (Table 1), as opposed to their spectral types (Oppenheimer et al. 2013; Route & Wolszczan 2013). Two surveyed exoplanets are within the habitable zones of their host stars: clockwise from upper left are HD 10697b and 55 Cnc f (Kane & Gelino 2012). The Jovian auroral decametric radio emission as measured by *Cassini* anchors the right plot in the lower right corner (Zarka et al. 2004).

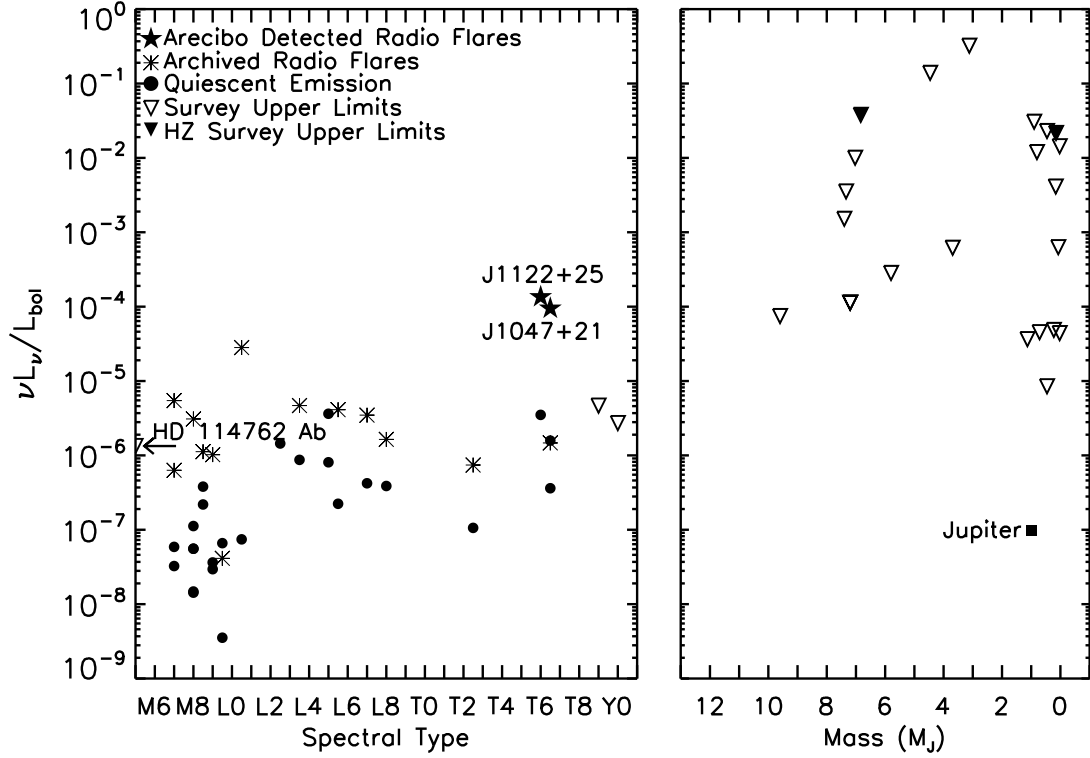


**Figure 3.** Logarithmic plots of radio luminosities as a fraction of bolometric luminosities versus spectral type (left panel) or exoplanet mass (right panel) of surveyed brown dwarf and low-mass stellar companions, as compared to previously detected radio-emitting UCDs (Burgasser et al. 2015; Route & Wolszczan 2016b; Route 2017a; Williams & Berger 2015; Williams et al. 2014, 2015, 2017; Zic et al. 2019; Richey-Yowell et al. 2020). The two radio-flaring, late T-type brown dwarfs, J1047+21 and J1122+25, near the brown dwarf/exoplanet boundary discovered by AO are denoted by filled stars. The upper limit for HD 114762 Ab (spectral type  $\sim$ M5) is in the left panel near the left-hand y-axis. Upper limits for HD 106252b ( $\sim$ T9) and HD 38529c ( $\sim$ Y0) appear in the left panel at right. The upper limits to the radio emission from the four young exoplanets of the HR 8799 system (Route & Wolszczan 2013) are graphed based on their properties in Tables 1 and 3, as opposed to their brown dwarf-like luminosities and spectral properties. 51 Peg b has the most similar limit on radio emission as a fraction of its bolometric luminosity ( $\nu L_\nu / L_{bol}$ ) to that of Jupiter and appears approximately two orders of magnitude above it. Two surveyed exoplanets are within the habitable zones of their host stars: clockwise from one o'clock are HD 10697b and 55 Cnc f (Kane & Gelino 2012). The Jovian auroral decametric radio emission relative to its cloud-top bolometric luminosity is represented by the square at lower right in the right panel (Zarka et al. 2004; Guillot 2005).